AD-A102 137 OHIO STATE UNIV COLUMBUS ELECTROSCIENCE LAB F/G 20/3
A HYBRID UTD-EIGENFUNCTION METHOD FOR SCATTERING BY A VERTEX.(U)
MAY 81 J N SAHALOS, G A THIELE F19628-78-C-0198
UNCLASSIFIED ESL-711353-3 RADC-TR-81-89 NL

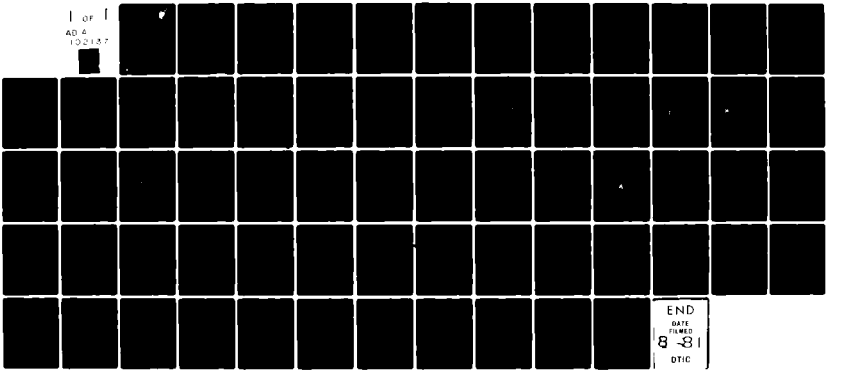

RADC-TR-81-89
Interim Report
May 1981

LEVEL II

12

A HYBRID UTD-EIGENFUNCTION METHOD FOR SCATTERING BY A VERTEX

The Ohio State University

J. N. Sahalos
G. A. Thiele

ROME AIR DEVELOPMENT CENTER
Air Force Systems Command
Griffiss Air Force Base, New York 13441

This report has been reviewed by the RADC Public Affairs Office (PA) and is releasable to the National Technical Information Service (NTIS). At NTIS it will be releasable to the general public, including foreign nations.

RADC-TR-81-89 has been reviewed and approved for publication.

APPROVED: Ronald G. Newburgh

RONALD G. NEWBURGH
Project Engineer

APPROVED: Allan C. Schell

ALLAN C. SCHELL
Chief
Electromagnetic Sciences Division

FOR THE COMMANDER: John P. Huss

JOHN P. HUSS
Acting Chief, Plans Office

If your address has changed or if you wish to be removed from the RADC mailing list, or if the addressee is no longer employed by your organization, please notify RADC (EECT) Hanscom AFB MA 01731. This will assist us in maintaining a current mailing list.

Do not return this copy. Retain or destroy.

UNCLASSIFIED

SECURITY CLASSIFICATION OF THIS PAGE (When Data Entered)

REPORT DOCUMENTATION PAGE

READ INSTRUCTIONS BEFORE COMPLETING FORM

1. REPORT NUMBER	2. GOVT ACCESSION NO.	3. RECIPIENT'S CATALOG NUMBER
RADC-TR-81-89	AD-A102437	

4. TITLE (and Subtitle)	5. TYPE OF REPORT & PERIOD COVERED
A HYBRID UTD-EIGENFUNCTION METHOD FOR SCATTERING BY A VERTEX	Interim Report
	6. PERFORMING ORG. REPORT NUMBER: ESL-711353-3

7. AUTHOR(s)	8. CONTRACT OR GRANT NUMBER(s)
J. N. Sahalos G. A. Thiele	F19628-78-C-0198

9. PERFORMING ORGANIZATION NAME AND ADDRESS	10. PROGRAM ELEMENT, PROJECT, TASK AREA & WORK UNIT NUMBERS
The Ohio State University Department of Electrical Engineering Columbus OH 43212	61102F 2305J432
11. CONTROLLING OFFICE NAME AND ADDRESS	12. REPORT DATE
Deputy for Electronic Technology (RADC/EECT) Hanscom AFB MA 01731	May 1981
	13. NUMBER OF PAGES: 68
14. MONITORING AGENCY NAME & ADDRESS(if different from Controlling Office)	15. SECURITY CLASS. (of this report)
Same	UNCLASSIFIED
	15a. DECLASSIFICATION DOWNGRADING SCHEDULE: N/A

16. DISTRIBUTION STATEMENT (of this Report)

Approved for public release, distribution unlimited

17. DISTRIBUTION STATEMENT (of the abstract entered in Block 20, if different from Report)

Same

18. SUPPLEMENTARY NOTES

RADC Project Engineer: Ronald G. Newburgh (EECT)

19. KEY WORDS (Continue on reverse side if necessary and identify by block number)

Scattering
Geometrical Theory of Diffraction
Eigenfunctions

20. ABSTRACT (Continue on reverse side if necessary and identify by block number)

Present solutions for the electromagnetic scattering by a vertex are either approximate or difficult to use for computations. For example, GTD solutions for vertex scattering are not yet fully developed and yield approximate results of unknown accuracy. The exact eigenfunction solution is both difficult to use and computationally inefficient due to the large number of eigenfunctions that must be retained.

DD FORM 1 JAN 73 1473 EDITION OF 1 NOV 65 IS OBSOLETE

UNCLASSIFIED

SECURITY CLASSIFICATION OF THIS PAGE (When Data Entered)

40225L

In this work, we obtain the scattering by a vertex (e.g., a quarter plane) by employing the exact eigenfunction solution only in a very small region close to the tip of the vertex (i.e., within 0.2λ). Thus, only a small number of eigenfunctions (e.g., two or three) are required to obtain the current in the top region. Outside of this region, the UTD is employed to obtain the current. The changeover point is determined by finding the point where the eigenfunction current has decayed to that predicted by UTD wedge diffraction theory.

Results will be shown for both the current on the quarter plane and also for the scattered field. In addition, the field scattered by a rectangular plate using this method will be compared with that predicted by the UTD with vertex diffraction, and the results will be seen to be in very close agreement.

TABLE OF CONTENTS

I. INTRODUCTION

Previous work on the problem of diffraction by a plane angular sector (see Figure 1) has been with the exact eigenfunction solution [1,2] but results have been presented for only the quarter plane (i.e., $k^2 = 1/2$). The eigenfunction solution, of course, requires a large number of terms to obtain a converged result and this, as well as the complexity of the solution, restricts its usefullness. As stated by Satterwhite [2], "the solution is general and needs some simplification before it can become a useful tool for diffraction studies."

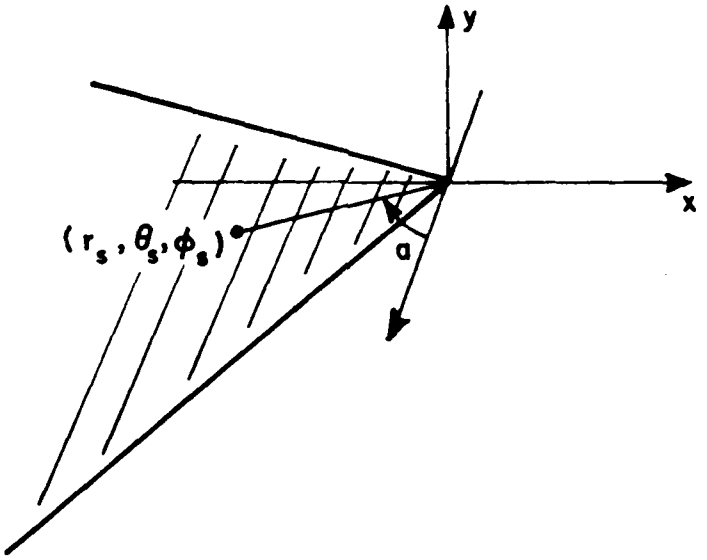

Figure 1.

The purpose of this paper is to make a simplification in the exact eigenfunction solution so that the solution may be more easily used. Not only are the eigenvalues found for the quarter plane as has been done previously, but the first few contributing eigenvalues

are found for almost any angular sector. These results are presented in graphical form for easy use.

The second purpose of this paper is to combine the eigenfunction solution with UTD wedge diffraction theory to obtain the current on the angular sector using only two or three eigenfunctions. The use of only a few eigenfunctions is possible because the eigenfunction solution is used to find the current only in the region very close (i.e., $r \approx 0.1\lambda$) to the vertex. The UTD is then used to determine the current everywhere else. By contrast, Satterwhite [2] used fifty eigenfunctions to calculate the current out to only one wavelength from the vertex.

Results will be shown for current distributions on angular sectors of various shapes (i.e., $0.1 \leq k^2 \leq 0.9$) and results will also be shown for the far field when the angular sector is illuminated by a short dipole. The angular sector will then be used along with superposition and the UTD to find the current on four-sided thin plates.

II. THE SPHERO-CONAL COORDINATE SYSTEM

The sphero-conal coordinate system is one of the few coordinate systems in which the vector wave equation is separable and it is in this system that the plane angular sector is a coordinate surface.

The sphero-conal system is described by three coordinate surfaces which are a sphere, an elliptic cone and an elliptic half-cone as illustrated in Figure 2. A plane angular sector is the $\theta=\pi$ coordinate surface of the sphero-conal system and its angle is determined by the ellipticity parameter k^2 of the system. The r,θ,ϕ coordinates are related with the cartesian x,y,z by the following equations:

$$x = r\cos\theta\sqrt{1 - k'^2\cos^2\phi}$$

$$v = r\sin\theta\sin\phi \tag{1}$$

$$z = r\cos\phi\sqrt{1-k^2\cos^2\theta}$$

where $k'^2 = 1-k^2$, $0 \leq k^2 \leq 1$, $0 \leq \theta \leq \pi$ and $0 \leq \phi \leq 2\pi$. The θ and ϕ angles are not the same as the angles of the spherical coordinate system. A point on the angular sector (Figure 1) has coordinates r_s, θ_s, ϕ_s where $\theta_s = \pi$ and $\phi_s = \cos^{-1}\left(\frac{\cos a}{k'}\right)$. The element ds of the surface on the angular sector is given by:

$$ds = r_s dr_s \frac{k' \sin\phi_s}{\sqrt{1-k'^2\cos^2\phi_s}} d\phi_s \quad . \tag{2}$$

The surface $\theta=\pi$ and $\phi=0$ as well as the surface $\theta=\pi$ and $\phi=\pi$ result in half planes. For a more detailed discussion of the sphero-conal system see Satterwhite [2] and Kraus and Levine [3,4].

III. EXACT SOLUTION FOR FIELDS AND THE ANGULAR SECTOR CURRENT DISTRIBUTION

The $\bar{E}$ field due to the current density $\bar{J}$ is determined by the dyadic Green's function which we must determine. The $\bar{E}$ field expression is of the form

$$\bar{E}(\bar{R}) = j\omega\mu \int_v \bar{\bar{\Gamma}}(\bar{R},\bar{R}').\bar{J}(\bar{R}')dv \quad . \tag{3}$$

$\bar{R}$ is a field point, $\bar{R}'$ is a source point and v is the source region. In Satterwhite's paper [1] we can see that the Green's function is given by

$$\bar{\bar{\Gamma}}(\bar{R},\bar{R}') = jk \sum_g \frac{\bar{M}^{II}_{g2}(\bar{R})\,\bar{M}^{I}_{g2}(\bar{R}')}{\Lambda_{g2}} + \frac{\bar{N}^{II}_{g1}(\bar{R})\,\bar{N}^{I}_{g1}(\bar{R}')}{\Lambda_{g1}} \tag{4}$$

$$\text{for } [\bar{R}] \geq [\bar{R}']$$

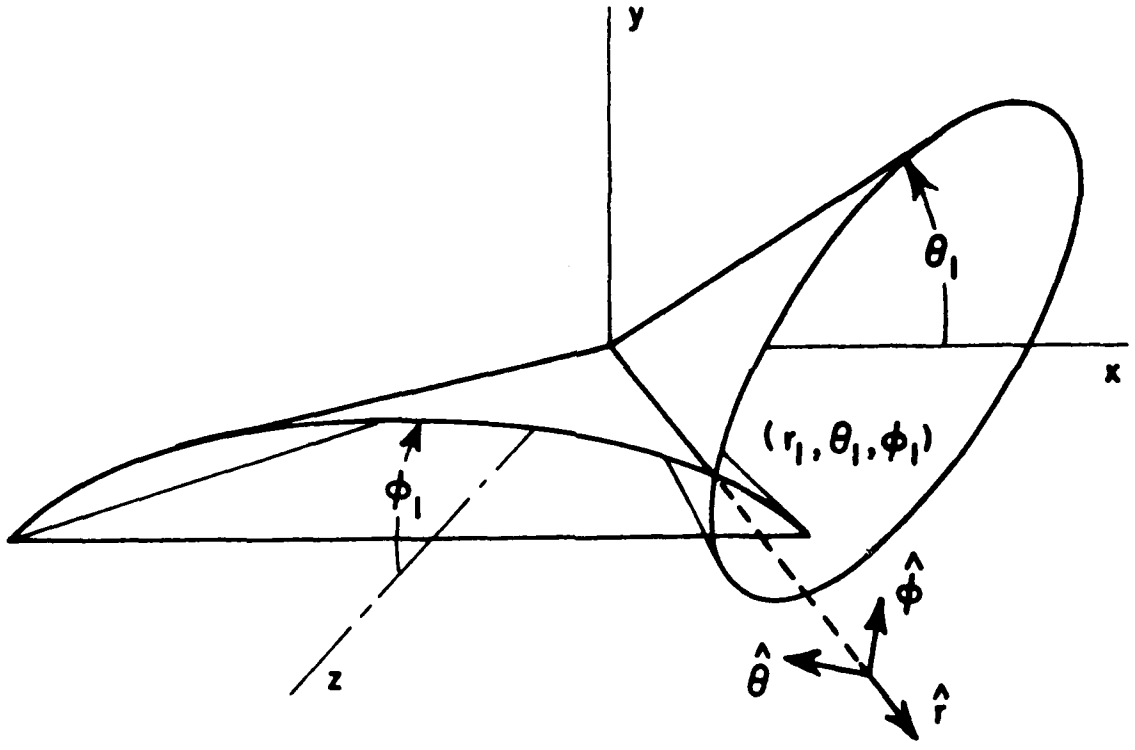

Figure 2. The sphero-conal coordinate system

and

$$\overline{\overline{\Gamma}}(\overline{R},\overline{R}') = j\kappa \sum_{g} \frac{\overline{M}^{I}_{g2}(\overline{R})\,\overline{M}^{II}_{g2}(\overline{R}')}{\Lambda_{g2}} + \frac{\overline{N}^{I}_{g1}(\overline{R})\,\overline{N}^{II}_{g1}(\overline{R}')}{\Lambda_{g1}} \qquad (5)$$

$$\text{for } [\overline{R}] \leq [\overline{R}']$$

where: κ is the wave number

g is the symbolic index which means the class of the odd or even solution of the problem

Λ_g is the normalization constant.

The vector wave functions are

$$\overline{M}_{g2} = \frac{Z_{vg2}(\kappa r)}{\sqrt{k^2\sin^2\theta + k'^2\sin^2\phi}}\left[\sqrt{1-k^2\cos^2\theta}\;\Theta'_{g2}(\theta)\,\Phi_{g2}(\phi)\hat{\phi} - \sqrt{1-k'^2\cos^2\phi}\;\Theta_{g2}(\theta)\,\Phi'_{g2}(\phi)\hat{\theta}\right] \qquad (6)$$

$$\overline{N}_{g1} = V_{g1}(V_{g1}+1)\frac{Z_{vg1}(\kappa r)}{(\kappa r)}\,\Theta_{g1}(\theta)\,\Phi'_{g1}(\phi)\,\hat{r} + \frac{[rZ_{vg1}(\kappa r)]'}{r\sqrt{k^2\sin^2\theta + k'^2\sin^2\phi}}\left[\sqrt{1-k'^2\cos^2\phi}\;\Theta_{g1}(\theta)\,\Phi'_{g1}(\phi)\,\hat{\phi} + \sqrt{1-k^2\cos^2\theta}\;\Theta'_{g1}(\theta)\,\Phi_{g1}(\phi)\hat{\theta}\right] . \qquad (7)$$

The $Z_v(\kappa r)$ function is the spherical Bessel Function where the superscript II means that

$$Z_v(\kappa r) = h_v^{(2)}(\kappa r) \qquad (8)$$

and the superscript I means that

$$Z_\nu(\kappa r) = j_\nu(\kappa r) \quad . \tag{9}$$

The $\Theta(\theta)$ and $\Phi(\phi)$ functions are Lamé functions defined by the scalar wave equations

$$\sqrt{1-k^2\cos^2\theta}\,\frac{d}{d\theta}\left(\sqrt{1-k^2\cos^2\theta}\,\frac{d\Theta}{d\theta}\right)+[(\nu(\nu+1)k^2\sin^2\theta+\mu]\Theta = 0 \tag{10}$$

and

$$\sqrt{1-k'^2\cos^2\phi}\,\frac{d}{d\phi}\left(\sqrt{1-k'^2\cos^2\phi}\,\frac{d\Phi}{d\phi}\right) + [(\nu+1)k'^2\sin^2\phi-\mu]\Phi = 0. \tag{11}$$

The two Equations (10) and (11) are coupled through the eigenvalues ν and μ. The $\bar{H}$ field is given by the curl of the $\bar{E}$ field as follows:

$$\bar{H}(\bar{R}) = \frac{j}{\omega\mu}\nabla\times\bar{E}(\bar{R}) = -\nabla \times \int_V \bar{T}(\bar{R},\bar{R}').\bar{J}(\bar{R}')dv \tag{12}$$

and the current of the angular sector is

$$\bar{J}(\bar{R}) = \hat{n}\times[\bar{H}(r,\theta=\pi,0<\phi<\pi) - \bar{H}(r,\theta=\pi,\pi<\phi<2\pi)] \quad . \tag{13}$$

IV. EIGENVALUES AND THE $\Theta(\theta)$ AND $\Phi(\phi)$ FUNCTIONS

From the above expressions we can see that we always need the first even and odd $\Theta(\theta)$ and $\Phi(\phi)$ functions and the eigenvalues associated with them. By using the infinite continued fraction method as in [1,2], the first three pairs of the main contributing eigenvalues μ and ν were found. These are plotted in Figure 3 where the ordinate is k^2 and the abscissa is either (ν or μ) for $0\leq\nu\leq 1.5$.

The general expressions for the $\Theta(\theta)$ and $\Phi(\phi)$ functions are

$$\Theta_e(\theta) = \Sigma\, A_m \cos(2m - \tfrac{1}{2})\theta \qquad (m=\ldots,-2,-1,0,1,2,\ldots) \tag{14}$$

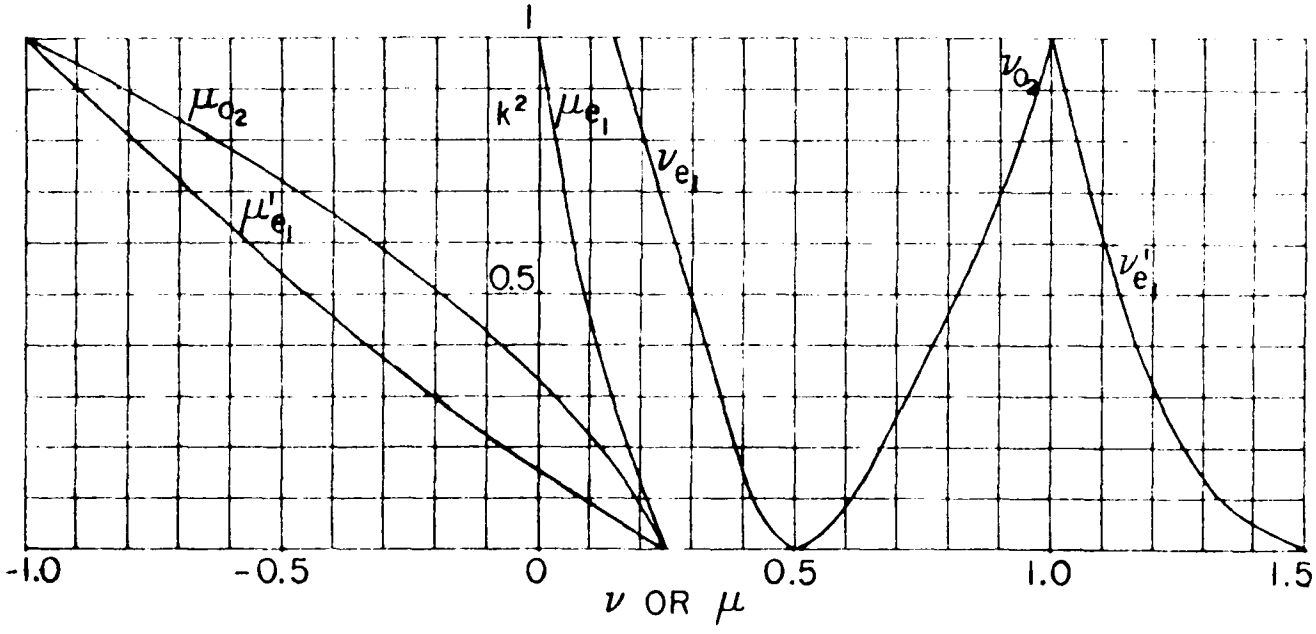

Figure 3. The first three ν and μ eigenvalues as a function of k^2.

$$\Theta_o(\theta) = \sum A_m \sin(2m - \tfrac{1}{2})\theta \qquad (m=\ldots,-2,-1,0,1,2,\ldots) \qquad (15)$$

$$\Phi_e(\phi) = \sum B_m \cos m\phi \qquad (m=0,1,2,3,\ldots) \qquad (16)$$

$$\Phi_o(\phi) = \sum B_m \sin m\phi \qquad (m=1,2,3,\ldots) \quad . \qquad (17)$$

Knowing the eigenvalues μ and ν, the coefficients A_m and B_m may be found for $0.1 \leq k^2 \leq 0.9$ by the continued fraction method used in [1,2] for the quarter plane ($k^2=1/2$) case. The procedure is tedious and laborious. The results are presented in Figures 4-9. The coefficients A_m and B_m may be determined from the figures with sufficient accuracy to use in Equations (12) and (13). Thus, with the aid of the figures, the current in a region close to the vertex may rather easily be determined for almost any angular sector as we shall see in the following sections.

V. $\bar{E}$ FAR ZONE FIELD APPROXIMATION FOR UNIT DIPOLE SOURCE LOCATED CLOSE TO THE TIP

An investigation of the eigenvalues ν and μ shows some interesting results. First we note that for any k^2

$$\nu_{1e1} < \nu_{1o2} < \nu_{2e1} \quad .$$

These three eigenvalues ν_{1e1}, ν_{1o2} and ν_{2e1} have values which vary from 0 to 1.5. If we examine Equations (6) and (7), we see that the functions $Z_\nu(\kappa r)$ and $\dfrac{[rZ_\nu(\kappa r)]'}{\kappa r}$ for $\kappa r \ll 1$ corresponding to the wave functions $\bar{M}^I$ and $\bar{N}^I$ become

$$Z_\nu(\kappa r) = j_\nu(\kappa r) = \frac{\sqrt{\pi}(\kappa r)^\nu}{2^{\nu+1}\,\Gamma(\nu+1.5)} \qquad (18)$$

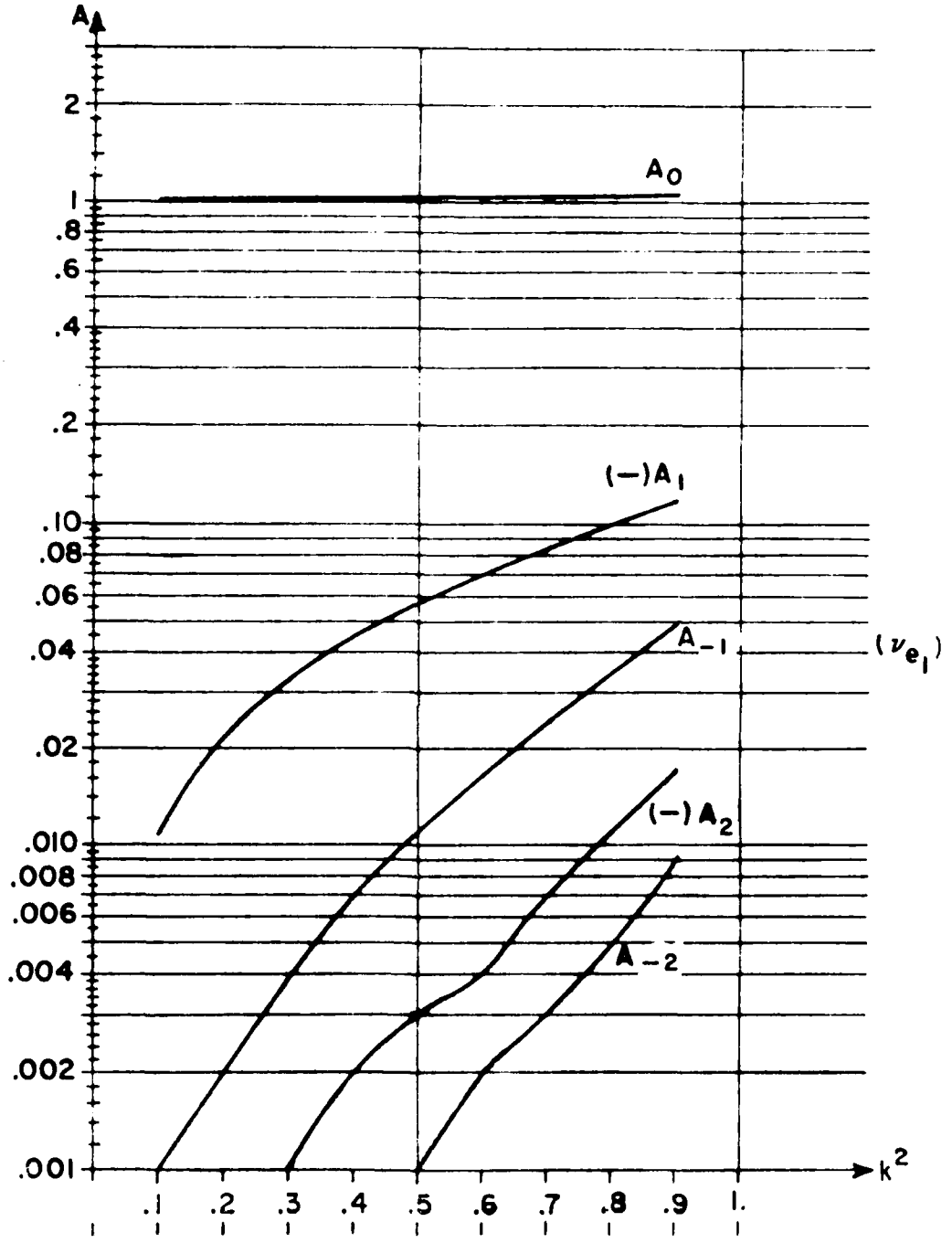

Figure 4. The A coefficients of the $\Theta(\theta)$ function for the first even solution.

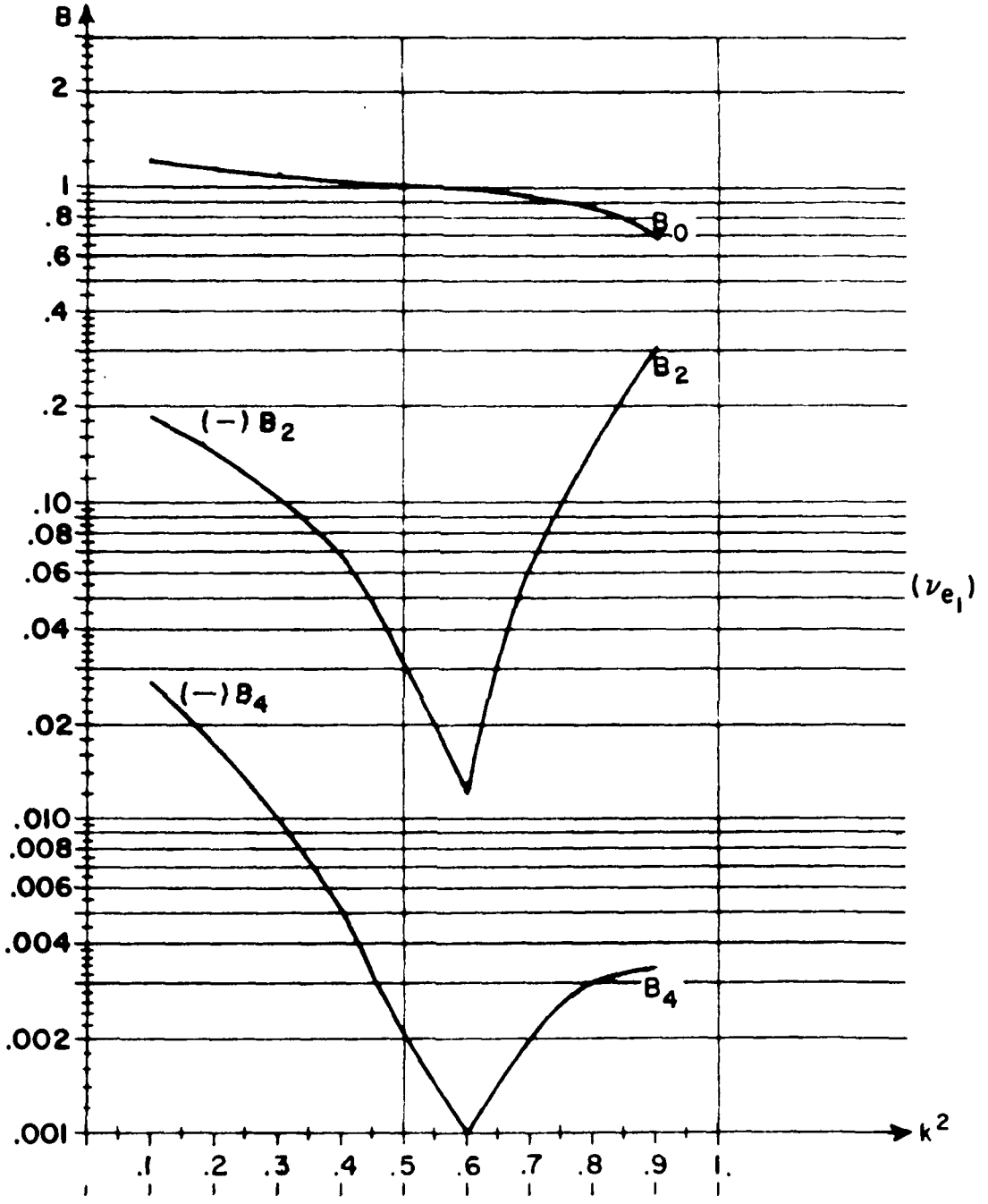

Figure 5. The B coefficients of the $\Phi(\phi)$ function for the first even solution.

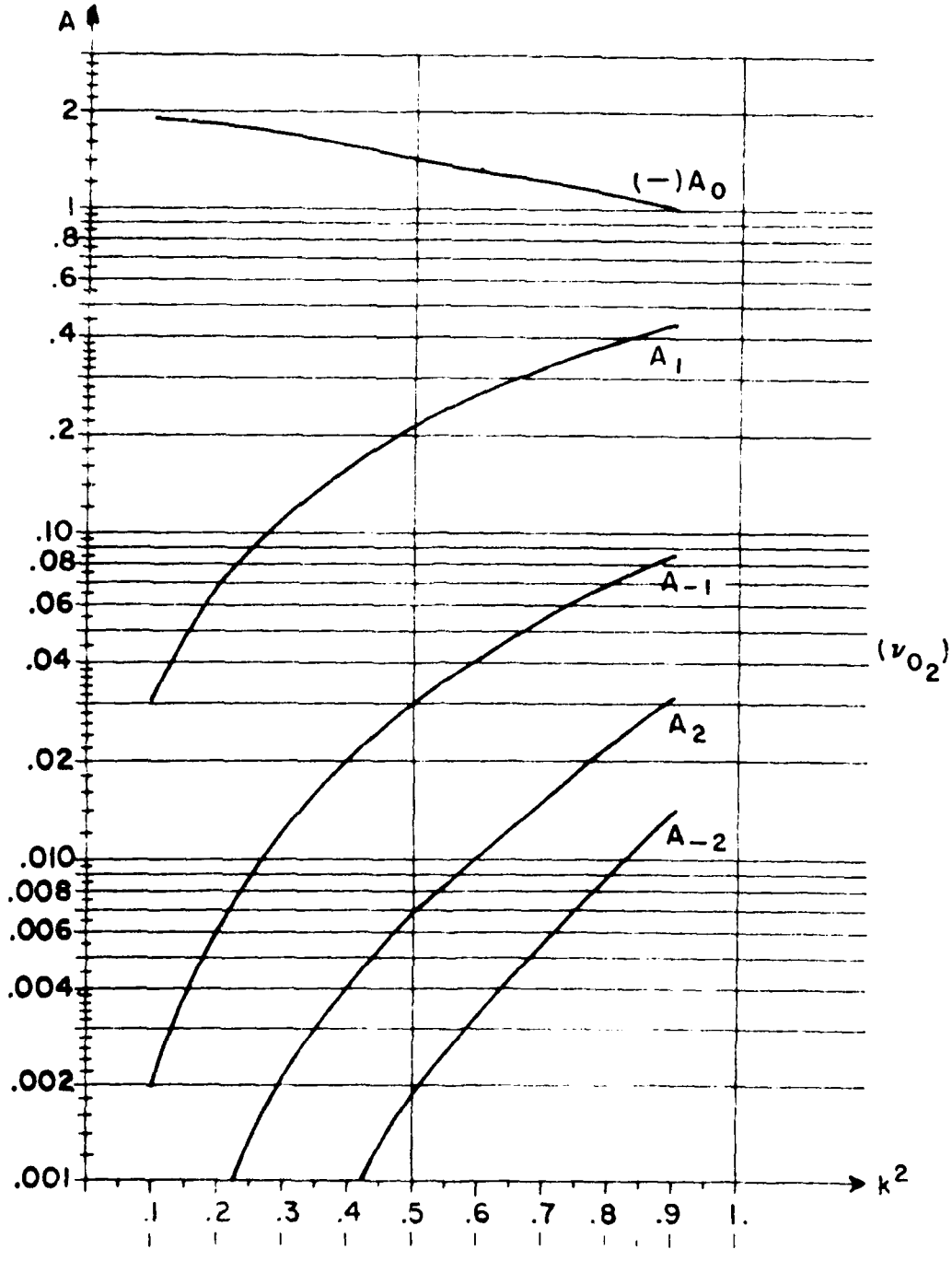

Figure 6. The A coefficients of the $\Theta(\theta)$ function for the first odd solution.

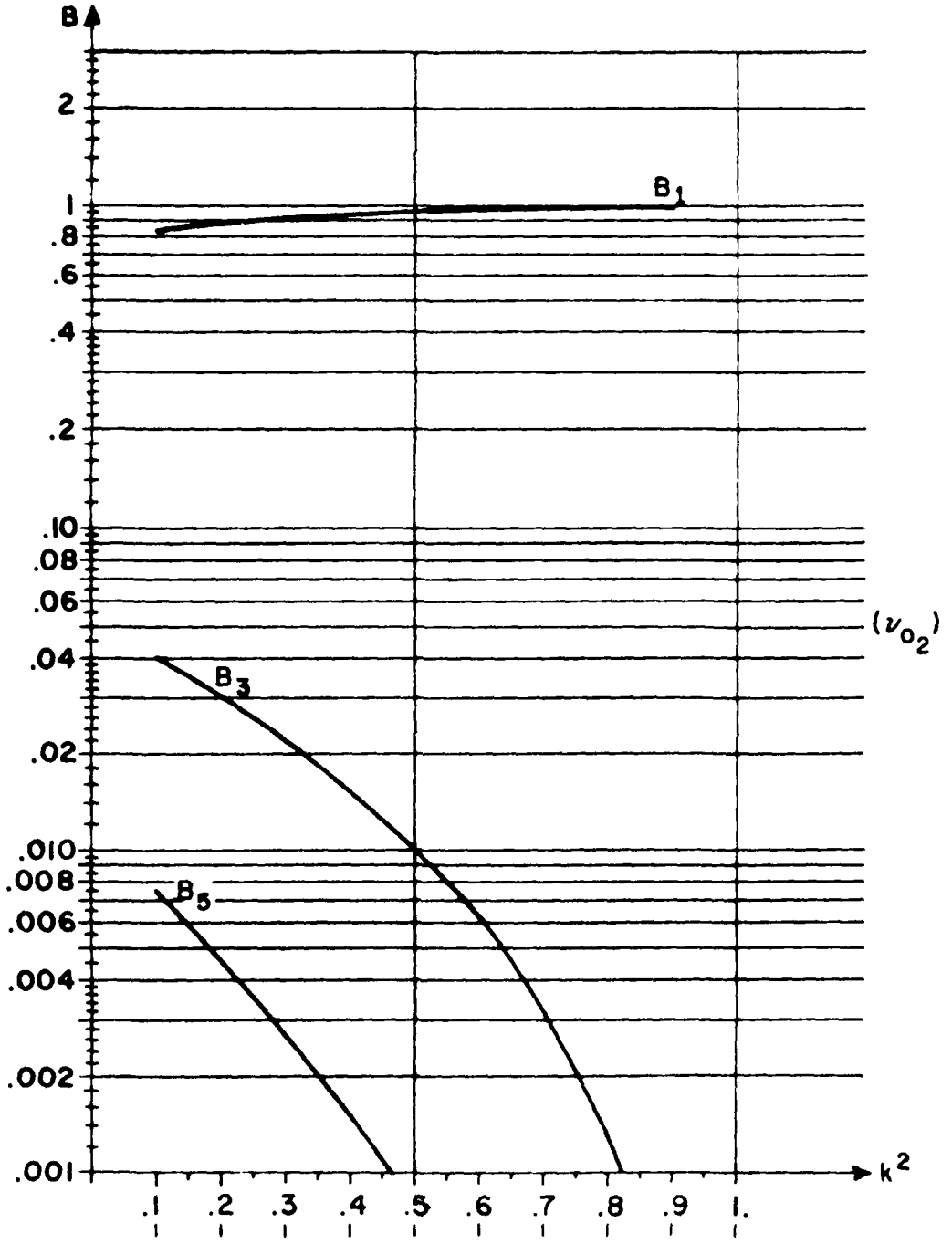

Figure 7. The B coefficients of the $\phi(\phi)$ function for the first odd solution.

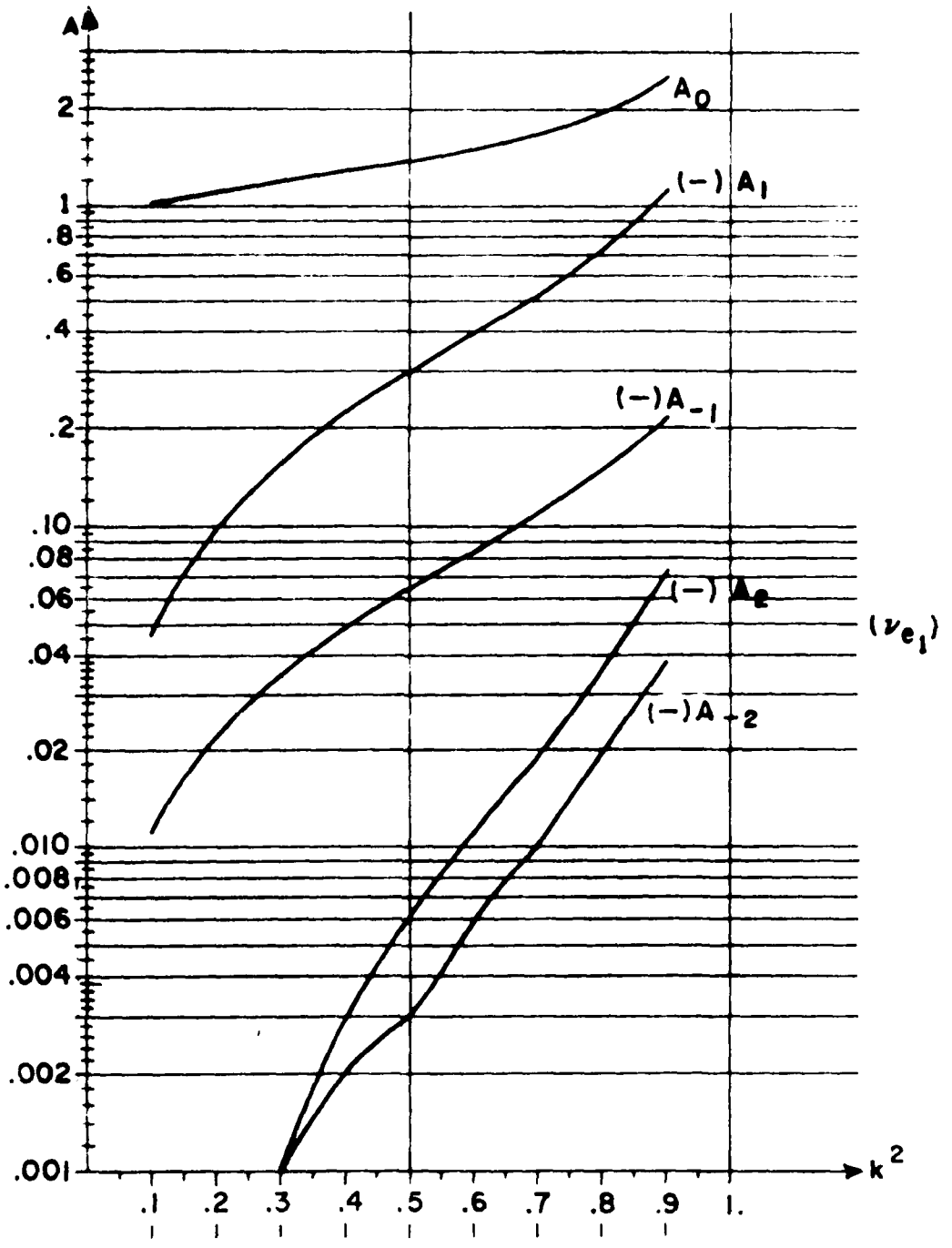

Figure 8. The A coefficients of the $\Theta(\theta)$ function for the second even solution.

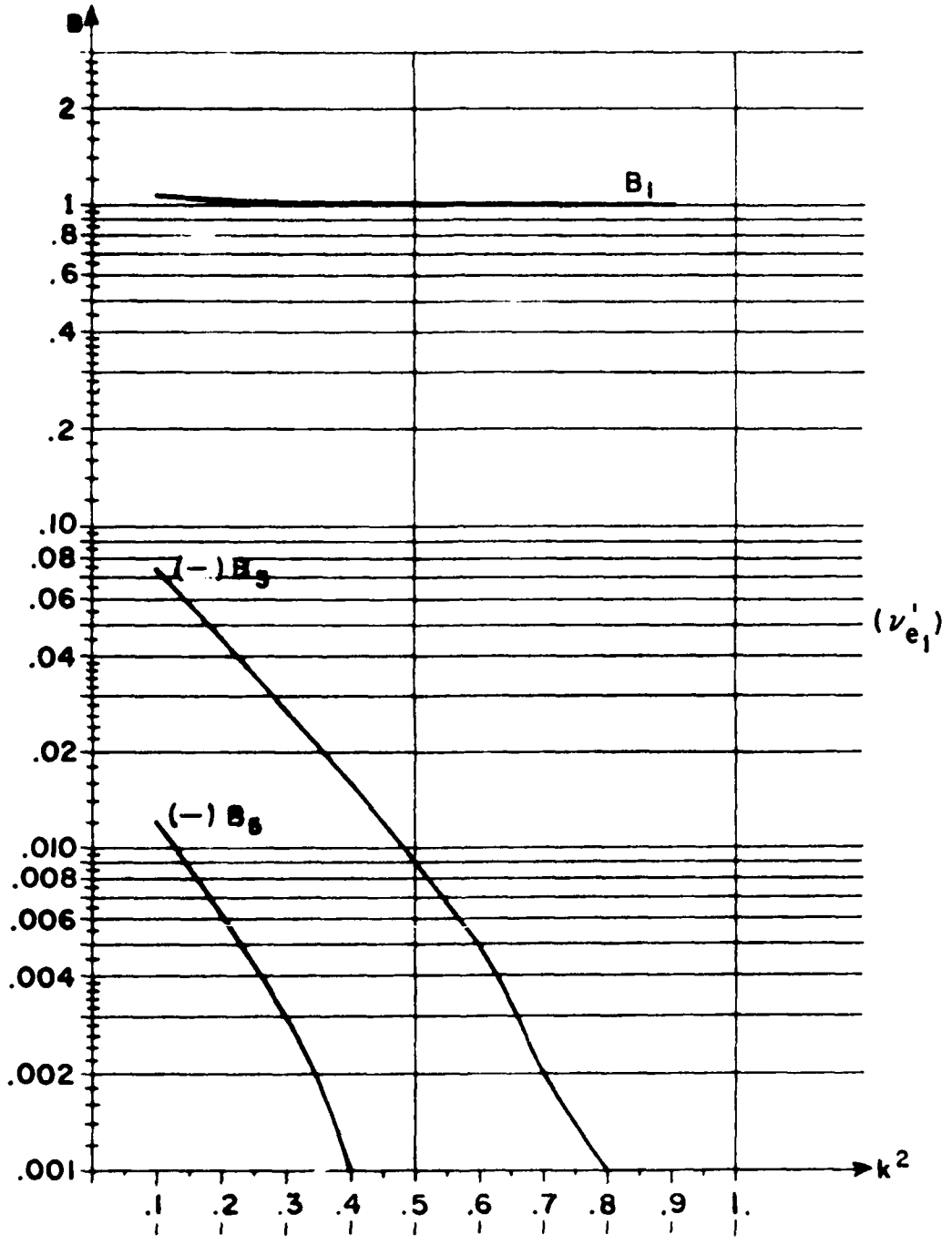

Figure 9. The B coefficients of the $\varsigma(\phi)$ function for the second even solution.

$$\frac{[rz_\nu(\kappa r)]'}{\kappa r} = \frac{[rj_\nu(\kappa r)]'}{\kappa r} \; \frac{\sqrt{\pi}(\nu+1)(\kappa r)^{\nu-1}}{2^\nu(2\nu+1)\Gamma(\nu+0.5)} \quad . \tag{19}$$

For small values of ν the expressions (18) and (19) are relatively larger than they are for big values of ν. This means that in the dyadic Green's function the first few terms, say three, have relatively big values compared to the others. So, when we want to get an approximate expression for the far zone electric field in the case of a unit dipole source located close to the vertex, we can use only the first few eigenvalues in the expression of the dyadic Green's function and obtain accurate results. In Figure 10 we see two locations of the unit dipole source. In Figures 11 to 15 we see the far zone electric field with $0.1 \leq k^2 \leq 0.9$, corresponding to Fig. 10a. In Figures 16 to 20 we see the far zone electric field for the second location of the unit source dipole. The computations in Figures 16 to 20 are for angular sectors with $0.1 \leq k^2 \leq 0.5$.

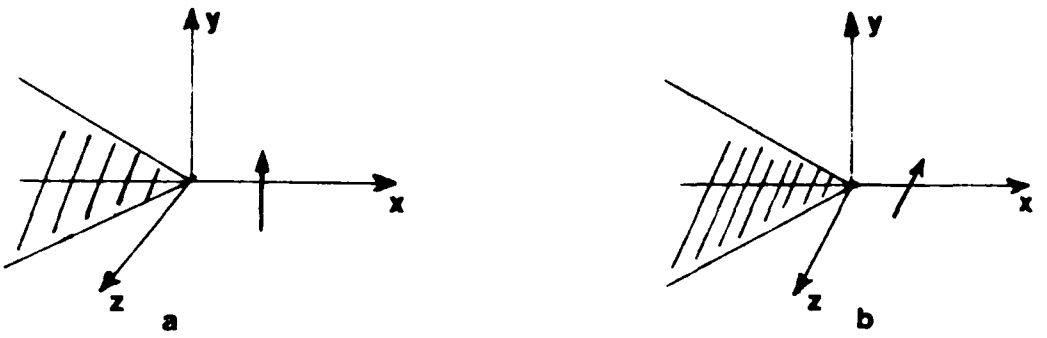

Figure 10.

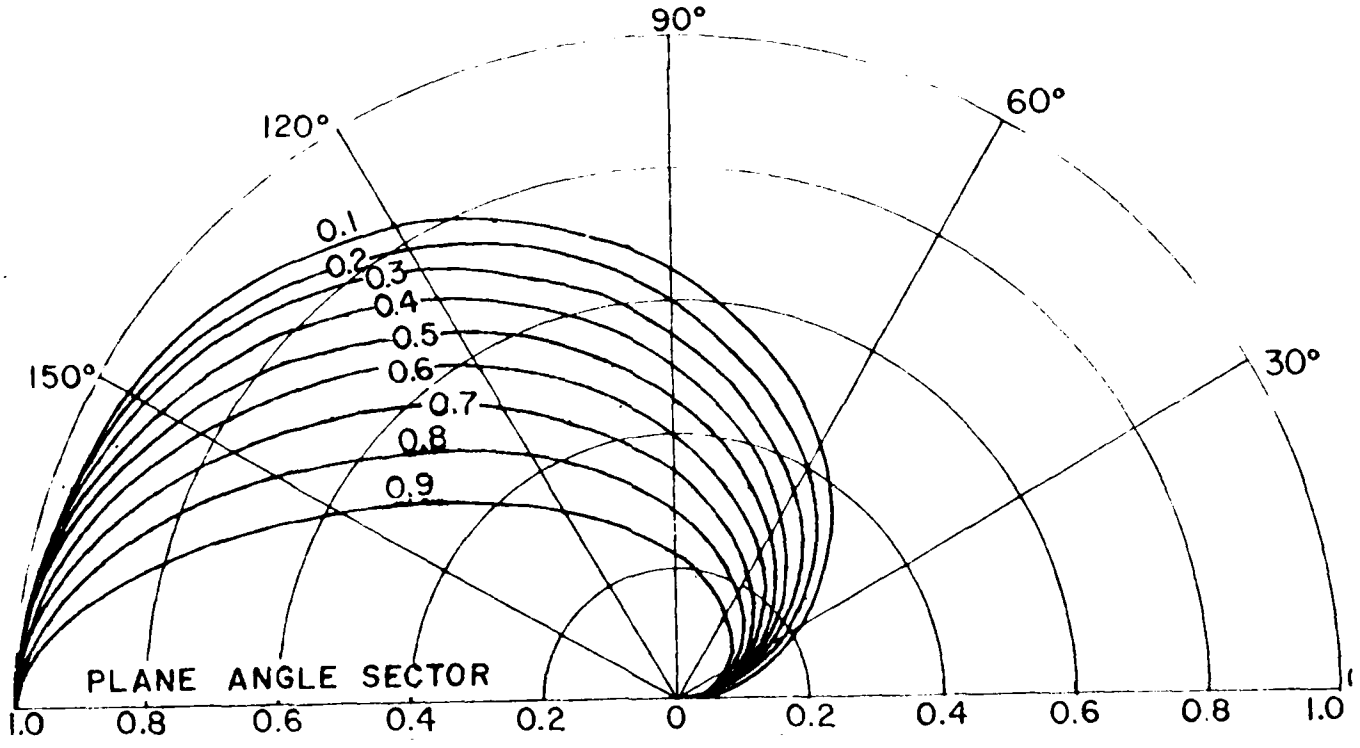

Figure 11. The Eθ far zone field in the z=o plane due to a unit source dipole close to the tip of plane angular sectors for k^2=0,1 to 0,9 (source on x axis and parallel to y).

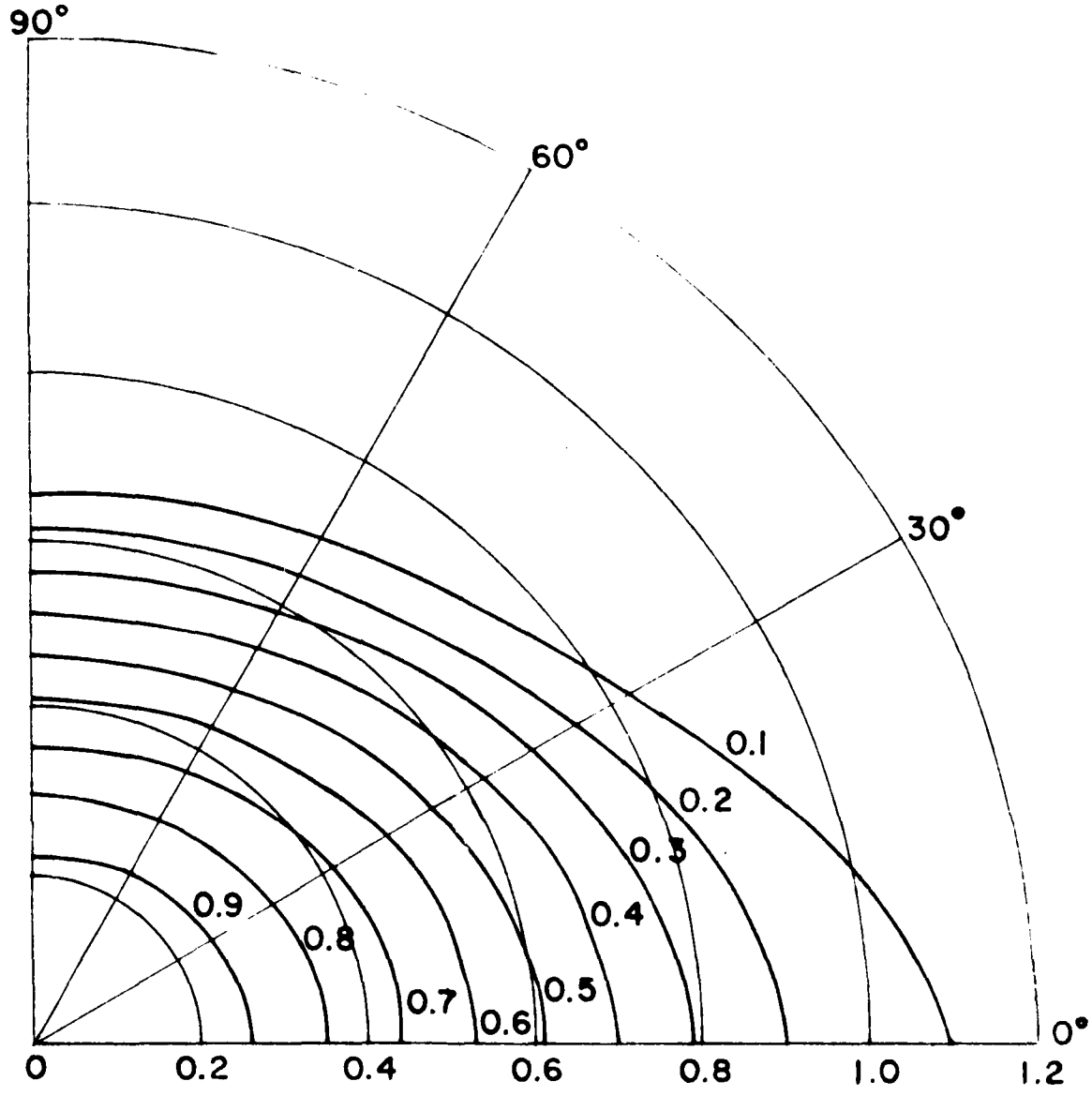

Figure 12. The E_θ far zone field in the x=o plane due to a unit source dipole close to the tip of plane angular sectors for k^2=0,1 to 0,9 (source on x axis and parallel to y).

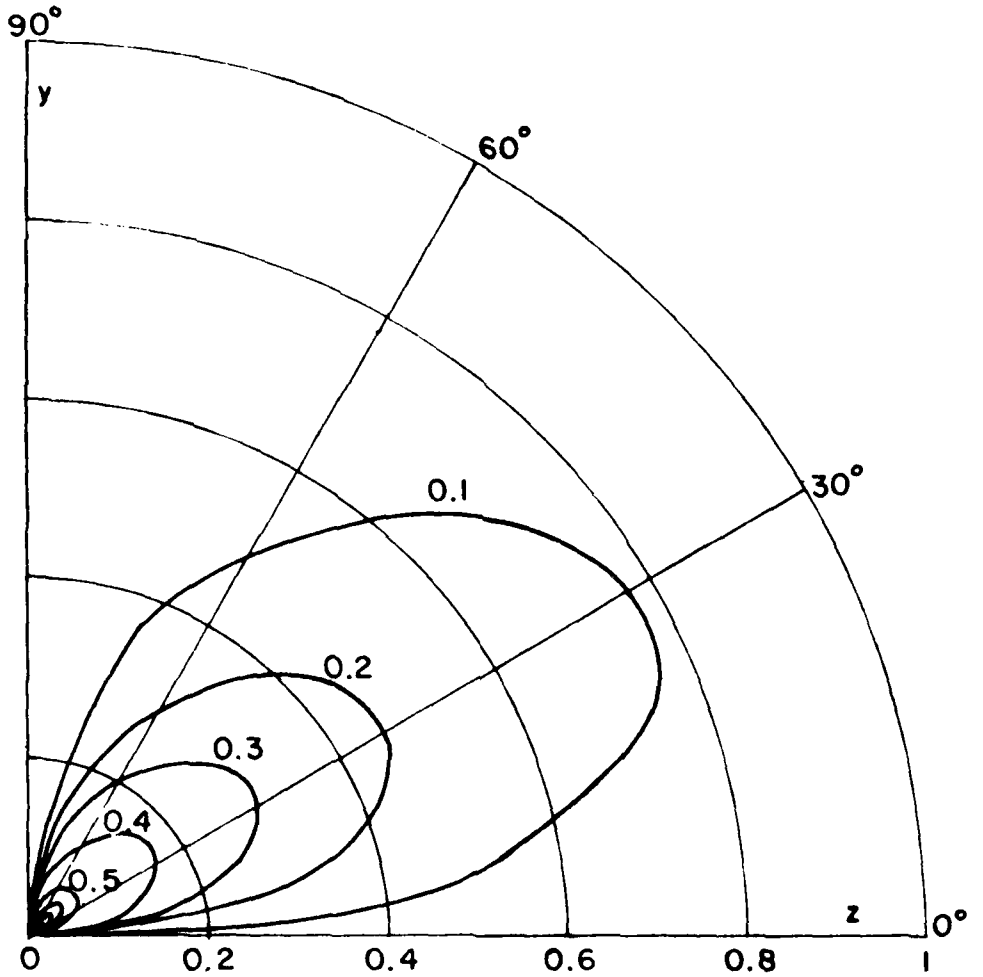

Figure 13. The E_ϕ far zone field in the x=o plane due to a unit source dipole close to the tip of plane angular sectors for k^2=0,1 to 0,9 (source on x axis and parallel to y).

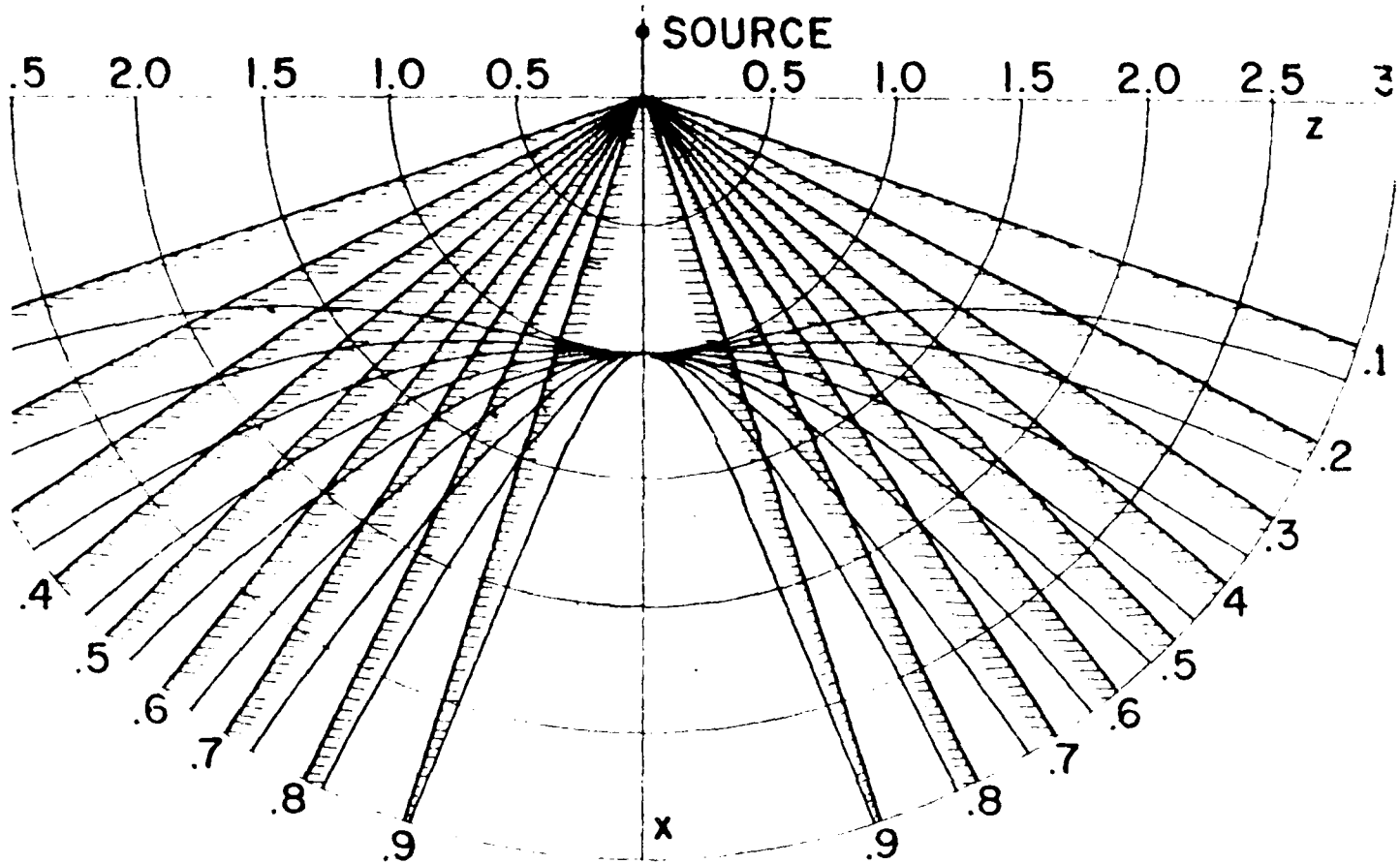

Figure 14. The Ee far zone field on the plane angular sectors due to a unit source dipole close to the tip for k^2=0,1 to 0,9 (source on x axis and parallel to y).

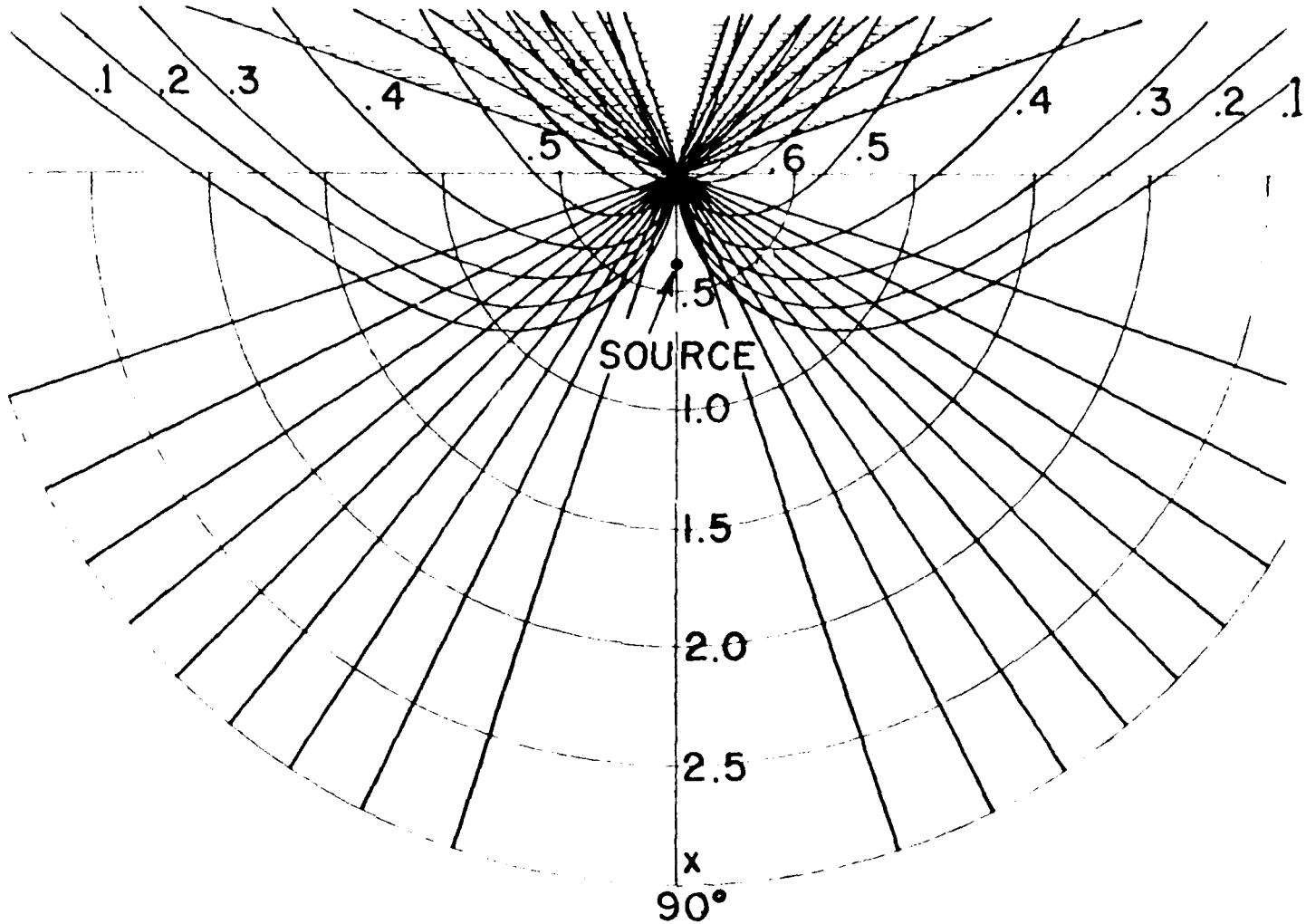

Figure 15. The E far zone field on tye y=o plane outside the angular sector due to a unit source dipole close to the tip for k^2=0,1 to 0,9 (source on x axis parallel to y).

VI. CURRENT DISTRIBUTION ON THE ANGULAR SECTOR

From Equation (13) it can be shown that the current distribution is:

$$\bar{J}(\bar{R}) = -2\kappa Y_o \sum_{\ell} \left\{ \frac{1}{\Lambda_{o2}} \int \bar{M}^{II}_{o2}(\bar{R}_o) \cdot \bar{J}(\bar{R}_o) dv \cdot A_{o2}(\pi) \right.$$

$$\left[-\nu_{o2}(\nu_{o2}+1) \frac{j_{\nu_{o2}}(\kappa r)}{\kappa r} \Phi_{o2}(\phi)\hat{\phi} + \frac{[r j_{\nu_{o2}}(\kappa r)]'}{\kappa r} \frac{1-k'^2\cos^2\phi}{k'\sin\phi} \Phi'_{o2}(\phi)\hat{r} \right] +$$

$$\left. + \frac{1}{\Lambda_{e1}} \int \bar{N}^{II}_{e1}(\bar{R}_o) \cdot \bar{J}(\bar{R}_o) dv \cdot A'_{e1}(\pi) \frac{j_{\nu_{e1}}(\kappa r)}{\sin\phi} \Phi_{e1}(\phi)\hat{r} \right\} \qquad (20)$$

$$\text{for } r \leq r_o$$

and

$$\bar{J}(\bar{R}) = -2\kappa Y_o \sum_{\ell} \left\{ \frac{1}{\Lambda_{o2}} \int \bar{M}^{I}_{o2}(\bar{R}_o \cdot \bar{J}(\bar{R}_o) dv \, \Theta_{o2}(\pi) \right.$$

$$\left[-\nu_{o2}(\nu_{o2}+1) \frac{h^{(2)}_{\nu_{o2}}(\kappa r)}{\kappa r} \Phi_{o2}(\phi)\hat{\phi} + \frac{[r h^{(2)}_{\nu_{o2}}(\kappa r)]'}{\kappa r} \frac{1-k'^2\cos^2\phi}{k'\sin\phi} \Phi'_{o2}(\phi)\hat{r} \right] + \alpha$$

$$\left. + \frac{1}{e1} \int \bar{N}^{I}_{e1}(\bar{R}_o) \cdot \bar{J}(\bar{R}_o) dv \cdot \Theta'_{e1}(\pi) \frac{h^{(2)}_{\nu_{e1}}(\kappa r)}{\sin\phi} \Phi_{e1}(\phi)\hat{r} \right\} \qquad (21)$$

$$\text{for } r \geq r_o \ .$$

The expressions indicate that the current in the $\hat{r}$ direction has the form $1/\sin\phi$. This means that the current on the edges goes to infinity. But we know the current distribution due to geometrical optics and the edge diffracted field does not give infinite current on the edges when the incident electric field is normal to the edge. So, we conclude that the $1/\sin\phi$ must arise because of the tip diffracted field.

Near the tip the current distribution is largely determined by the spherical Bessel function $J_\nu(\kappa r)$ when the source is within a distance $r_o \geq r$. For $\kappa r << 1$ the expression of the current will depend on the $j_\nu(\kappa r)$ which have small values of ν. As mentioned earlier, the small eigenvalues are the first two or three. These give the dominant current near the tip. With the help of Equation (13) for the even eigenfunctions the current distribution is

$$\bar{J}_{e1} = B(\kappa r)^{\nu_{e1}} \frac{\Phi_{e1}(\phi)}{\sin\phi}\hat{r} \tag{22}$$

and for the odd eigenvalues it is

$$\bar{J}_{o2} = A(\kappa r)^{\nu_{o2}-1}\left[-\Phi_{o2}(\phi)\hat{\phi} + \frac{1}{\nu_{o2}}\frac{\sqrt{1-k'^2\cos^2\phi}}{k'\sin\phi}\Phi'_{o2}(\phi)\hat{r}\right] \tag{23}$$

where

$$B = -2kY_o \frac{\pi\Theta'_{e1}(\pi)}{2^{\nu_{e1}+1}\Gamma(\nu_{e1}+1.5)\Lambda_{e1}} \int_v \bar{N}^{II}_{e1}(\bar{R}').\bar{J}(\bar{R}')dv \tag{24}$$

and

$$A = -2kY_o \frac{\pi\nu_{o2}(\nu_{o2}+1)\Theta_{o2}(\pi)}{2^{\nu_{o2}+1}\Gamma(\nu_{o2}+1.5)\Lambda_{o2}} \int_v \bar{M}^{II}_{o2}(\bar{R}').\bar{J}(\bar{R}')dv \tag{25}$$

Y_o is the free space admittance. From the expressions of the current near the tip we can see in general that the current depends on three different functions.

In Figures 16, 17 and 18 we can see the form of those functions for an angular sector with $k^2=0.3$. Far from the tip ($\kappa r > 1$) the tip diffracted current must be given by:

$$\bar{J}_{TD}(\bar{R}) = \frac{e^{-jkr}}{r}\left[\frac{\Phi_1(\phi)}{\sin\phi}\hat{r} + \Phi_2(\phi)\hat{\phi}\right] \tag{26}$$

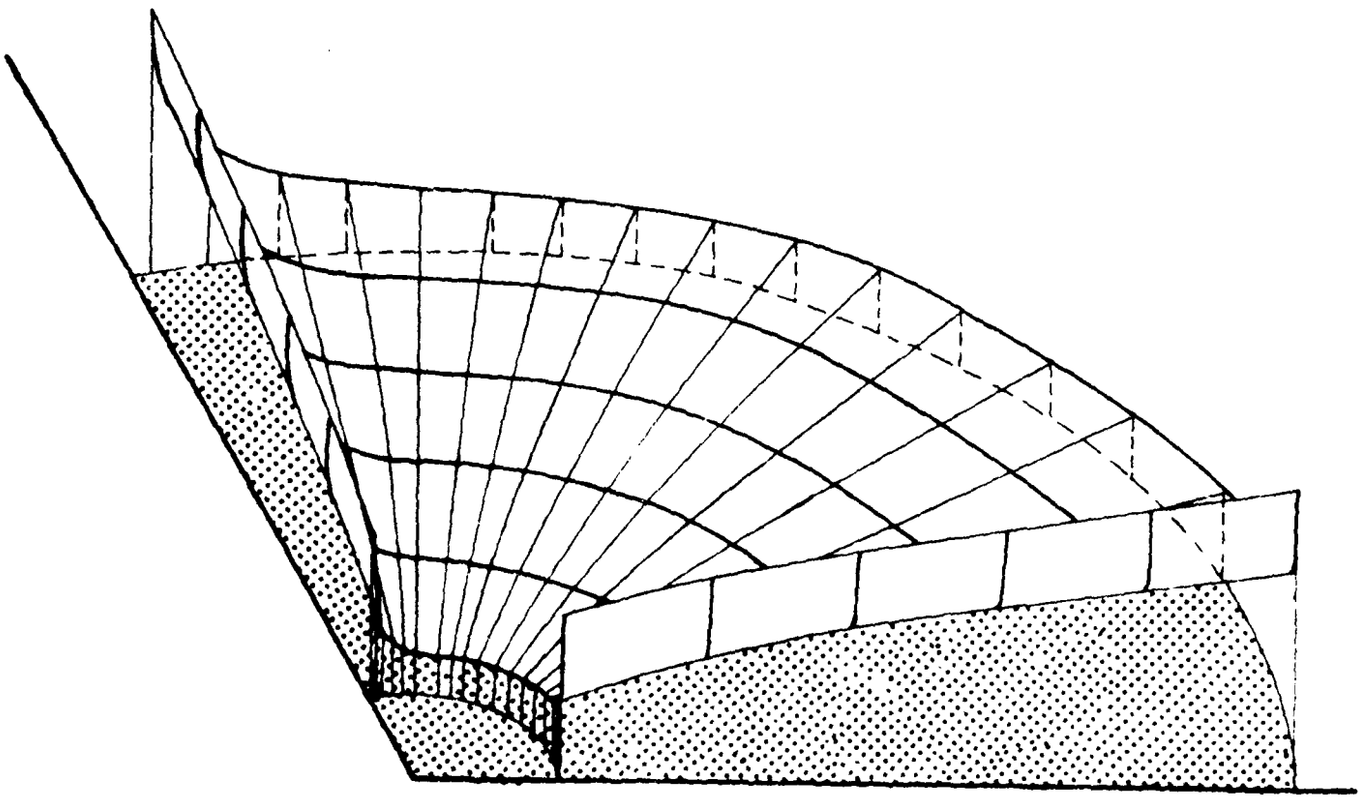

Figure 16a. The $J_r=(kr)^{\nu_{e_1}} \frac{\Phi_{e1}(\phi)}{\sin\phi}$ current distribution for an angular sector with $k^2=0.3$.

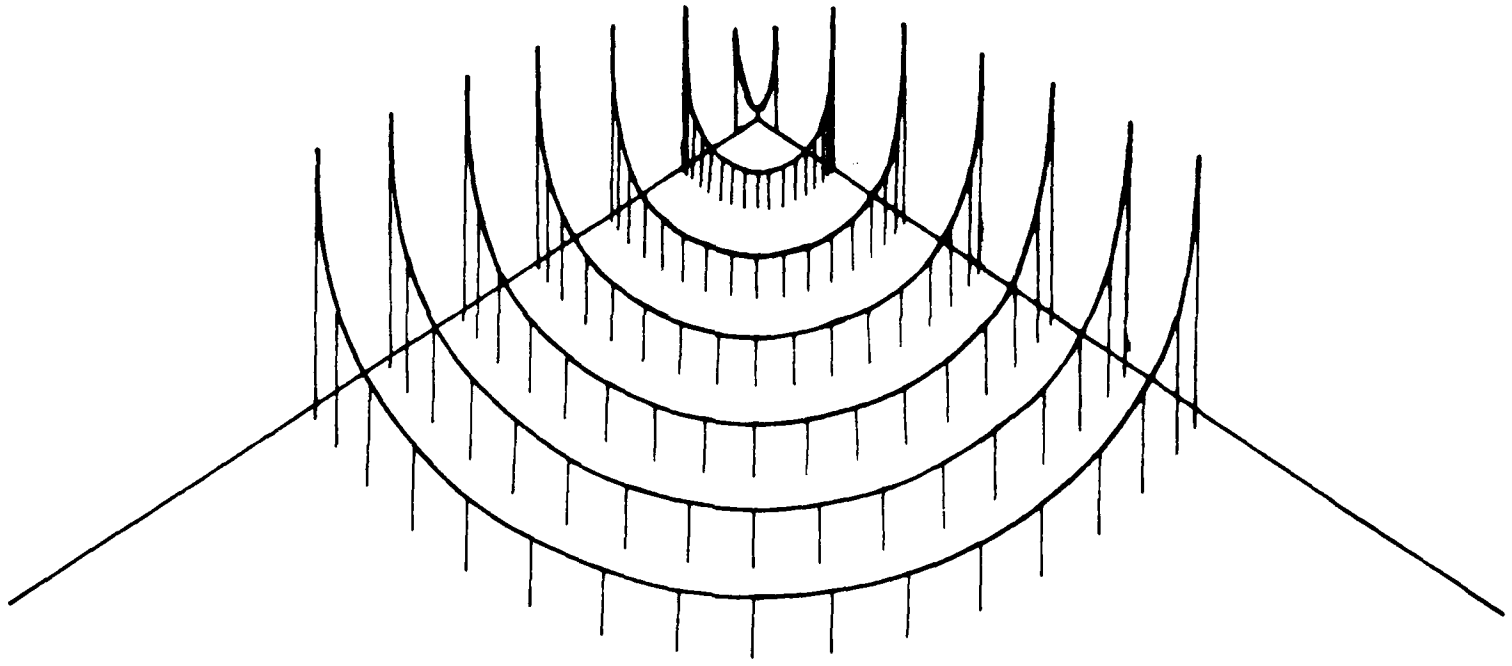

Figure 16b. The J_r current distribution as in Fig. 16a. as seen from a different aspect.

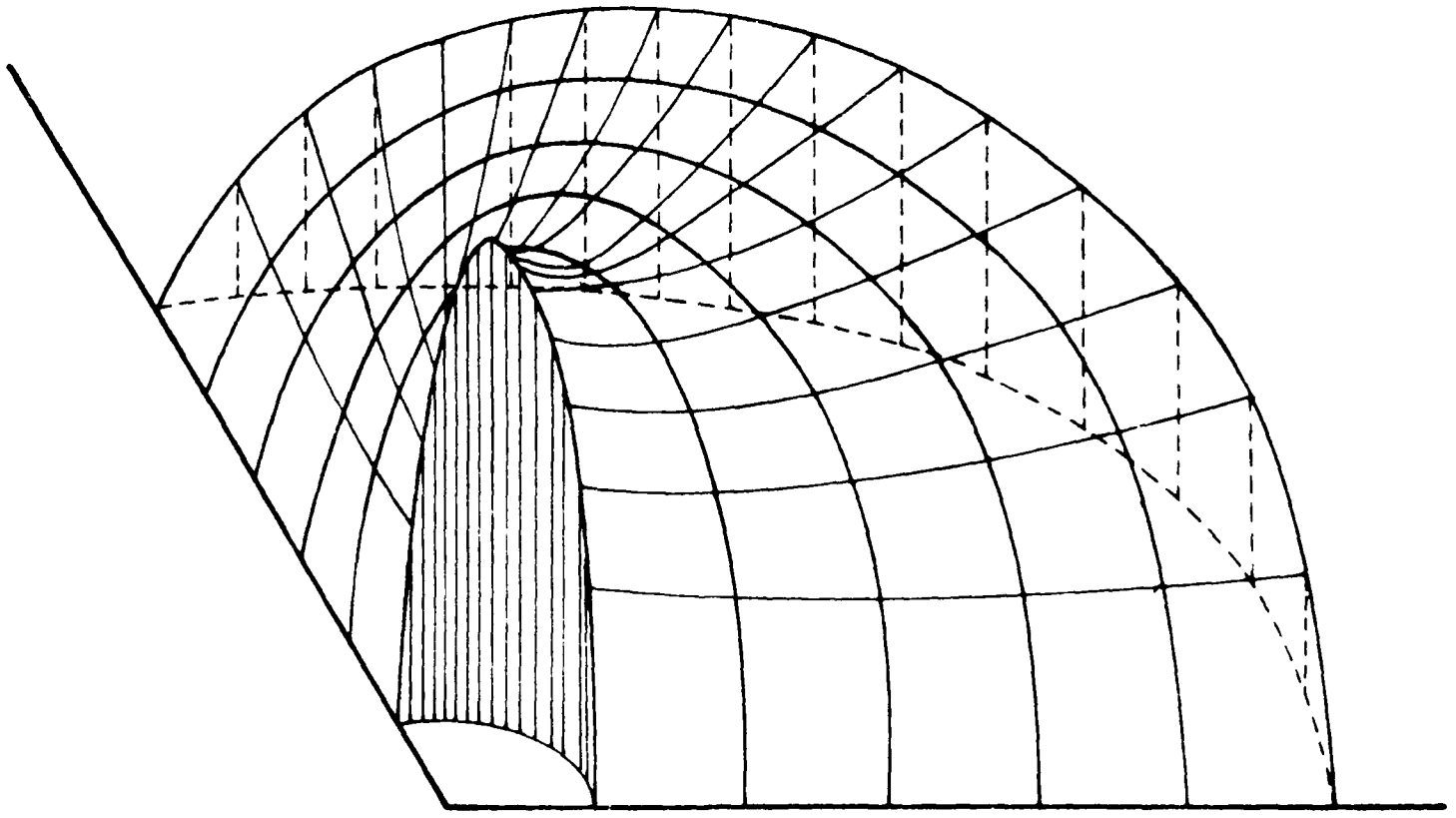

Figure 17a. The $J_{\nu}=(kr)^{\nu_{02}-1}\ \Phi_{02}(\phi)$ current distribution for an angular sector with $k^2=0.3$.

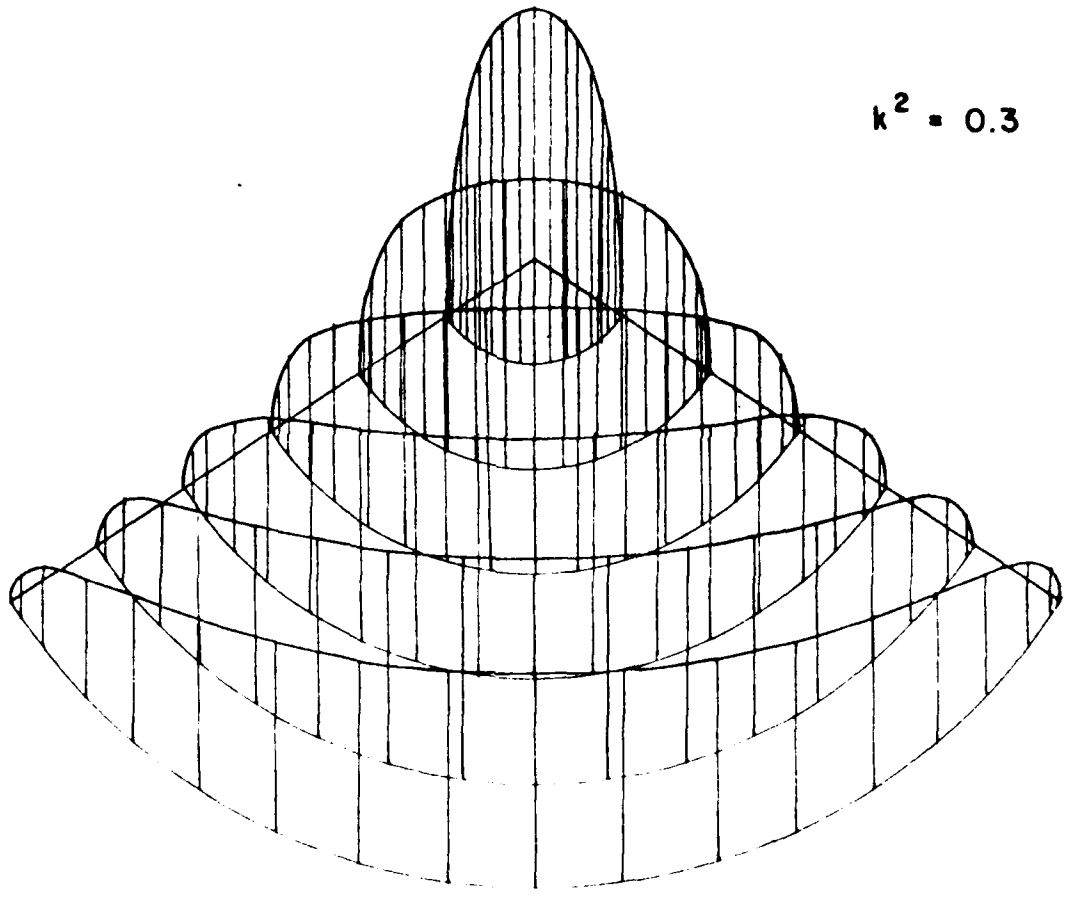

Figure 17b. The J_ϕ current distribution as in Fig. 17a as seen from a different aspect.

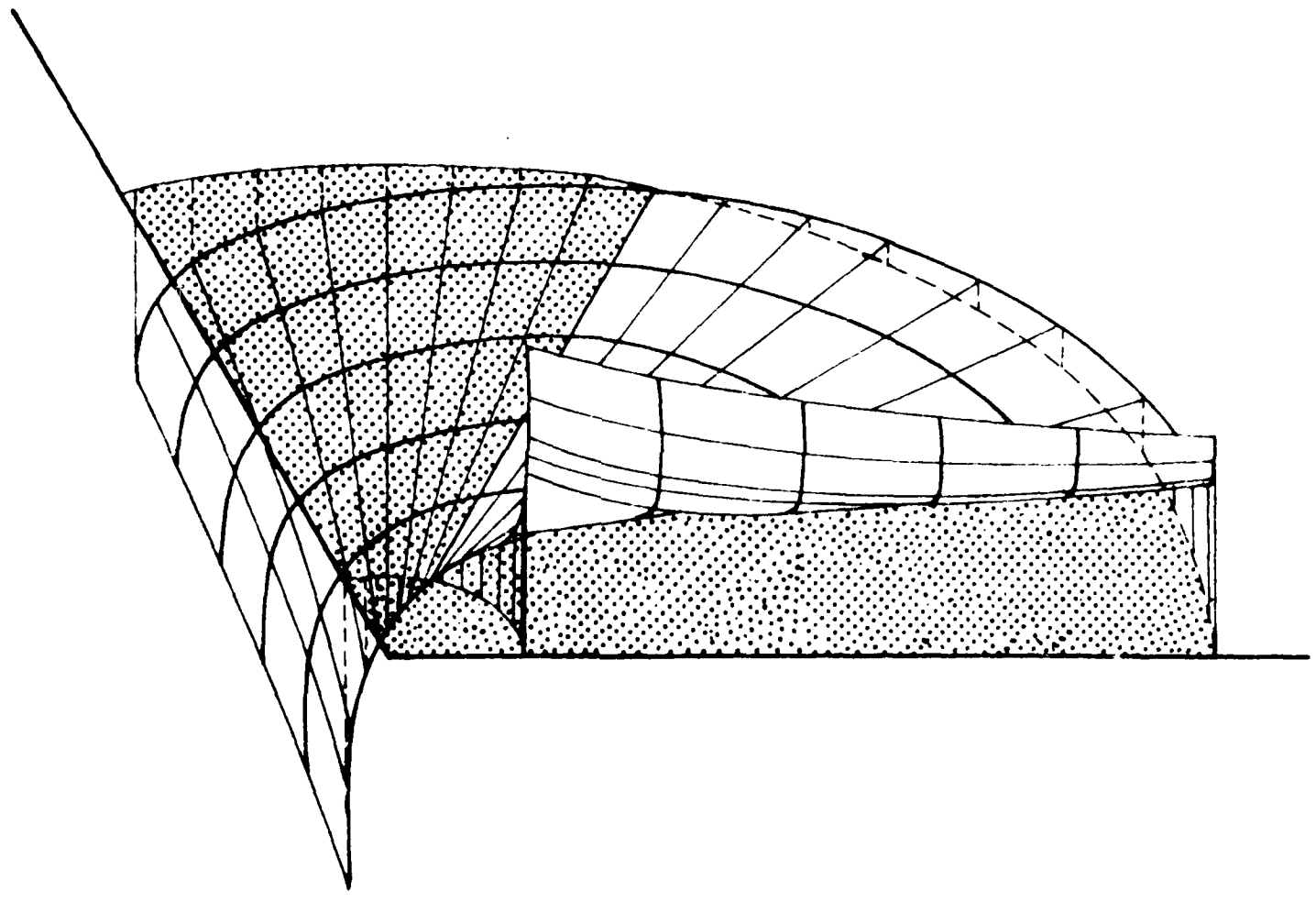

Figure 18a. The $J_r = \frac{1}{V_{o_2}} \frac{\sqrt{1-k'^2\cos^2\phi}}{k'\sin\phi} \phi'_{o2}(\phi)$ current distribution for an angular sector with $k^2=0.3$.

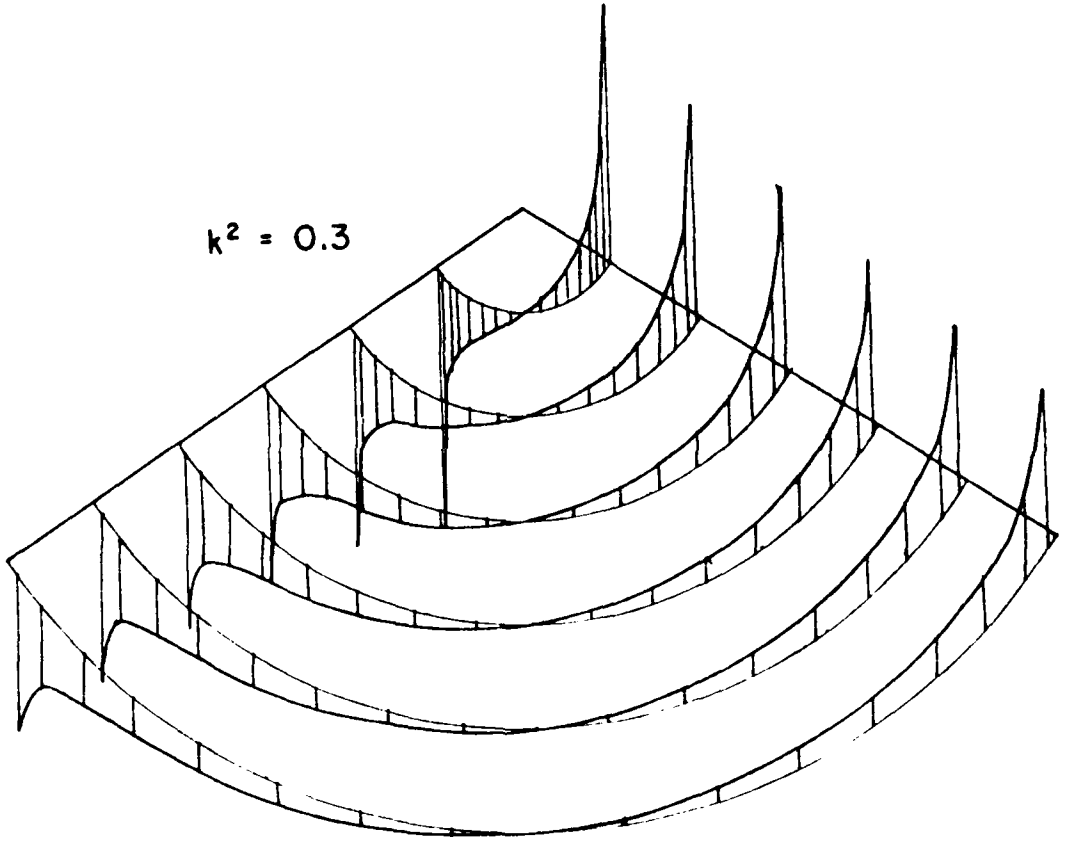

Figure 18b. The J_r current distribution as in Fig. 18a as seen from a different aspect.

where the functions $\Phi(\phi')$ are:

$$\Phi_1(\phi') = A_0+A_1\cos\phi+A_2\cos 2\phi+\ldots \tag{27}$$

$$\Phi_2(\phi) = B_0+B_1\sin\phi+B_2\sin 2\phi+\ldots \tag{28}$$

The unknown coefficients A_i and B_i can be found by using the EFIE to generate two systems of linear equations using point-matching. The EFIE is

$$\hat{n} \times \vec{E}^{inc}(\hat{r}) = \frac{1}{4\pi j\omega\epsilon}\,\hat{n} \times \int_S (-\omega^2\mu\epsilon\vec{J}_s G+\nabla'_s \vec{J}_s\nabla' G)dS \tag{29}$$

where G is the free space Green's function and $\vec{J}_s$ in this problem is given by

$$\left.\begin{aligned} \vec{J}_s &= \vec{J}_{total} && 0 \le \kappa r<1 \text{ (see Eq. (20)} \\ \vec{J}_s &= \vec{J}^{GO} + \vec{J}^{d}_{edges} + \vec{J}_{TD} && \kappa r \ge 1 \end{aligned}\right\} \tag{30}$$

or in words for $\kappa r<1$, the current is the sum of the geometrical optics current, the diffracted current from the edges and the tip diffracted current respectively.

VII. ANGULAR SECTOR FAR FIELD RESULTS

By using the EFIE with just three sample points, we found the three unknowns in the tip diffracted current expressions in Equations (27) and (28). The integration of EFIE was terminated 20 wavelengths from the sample point since the integrated functions go quickly to zero with distance. The sample points are typically located about 10λ from the tip. In Figures 19, 20, and 21 we can see the total field for an infinitesimal dipole located near the angular sector and normal to it. The distance of the dipole from the tip is $\kappa r_0 = 2.0$ with $\theta_0 = \pi$ and $\phi_0 = \pi/2$.

VIII. FINITE THIN PLATES

A finite thin plate has both edges and vertices. We can use the angular sector solution in section VI to obtain the currents in the regions close to the vertices and the UTD to obtain the currents elsewhere. If the vertices are far apart by more than a wavelength or so, we can neglect the interaction between the vertices and use the expressions in Sections VI and VII plus superposition to obtain the total contribution from the vertices. That is, we use the EFIE as in the previous section, except that the number of sample or match points will be n times the number of unknowns used in the angular sector case.

Results for a 3λ by 3λ square plate are shown in Figure 22. Due to the nature of our solution we see a large "spike" of current at the four corners in Figure 22a. The current in Figure 22a may be compared with that presented by Ko and Mittra [5], and it will be seen that the results are significantly different at the four corners since their results show no singularity of the current at the corners for this size plate. We believe, that because the interaction between corners is small (or negligible) for large plates, it is inevitable that a strong singularity be observed in current there. This conclusion is the opposite of that in [5]. It may be that the solution in [5] is not converged for large plates.

Figure 23 shows the current on a 3λ by 3λ plate that is not square, but in the shape of a rhombic with two corners characterized by $k^2=0.3$ and the other two by $k^2=0.7$. In both Figs. 22 and 23 the edge condition of the current is not shown for purposes of clarity nor is it used in the far field computation in the next paragraph.

Finally, Figure 24 shows the far field pattern of a short monopole or stub radiator at the center of a 8λ square ground plane. The result is compared with an unpublished result by Marhefka who obtained his result using the UTD with vertex diffraction. The two results are seen to be in very close agreement.

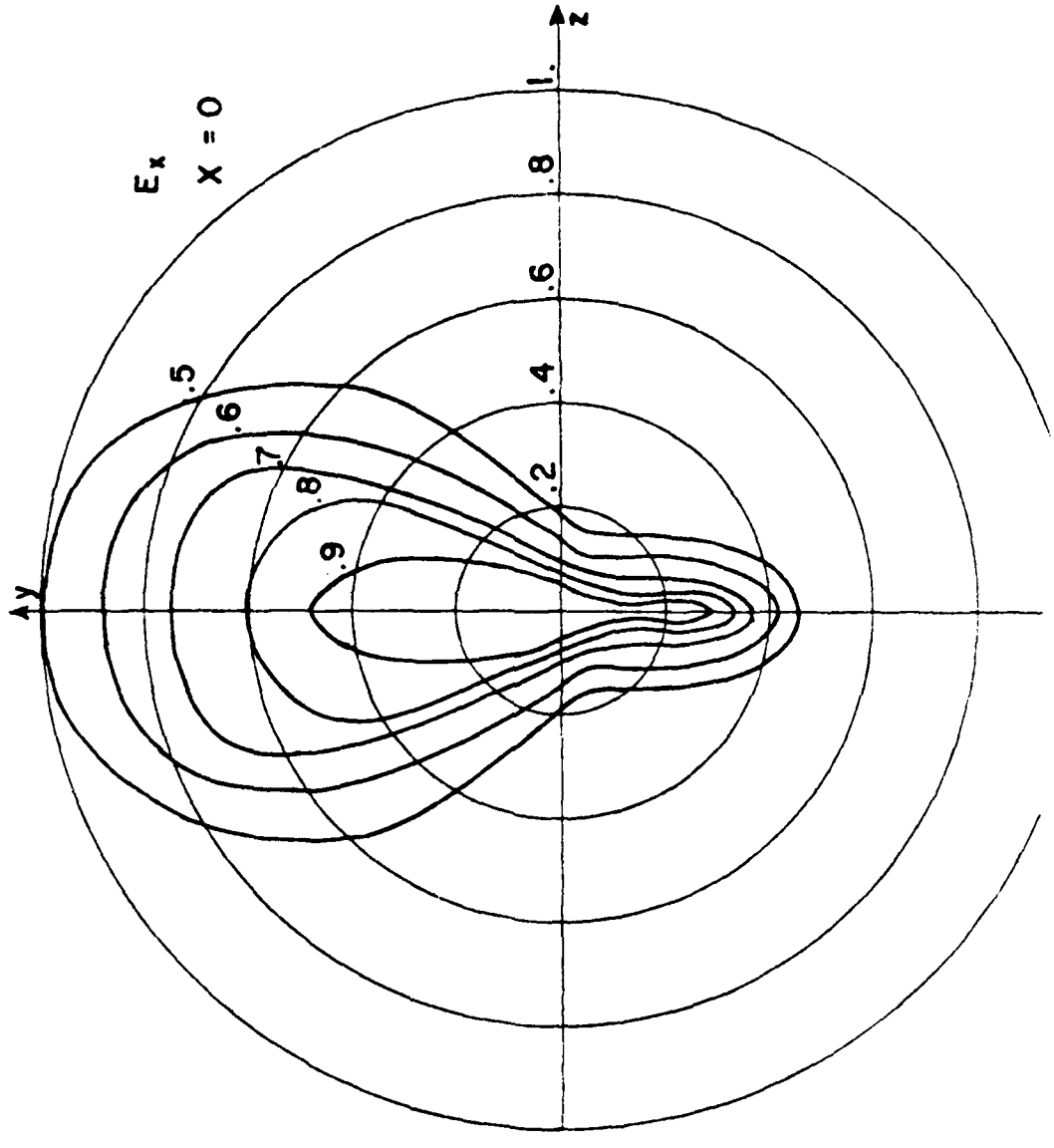

Figure 19. Total electronic field for five different angular sectors.

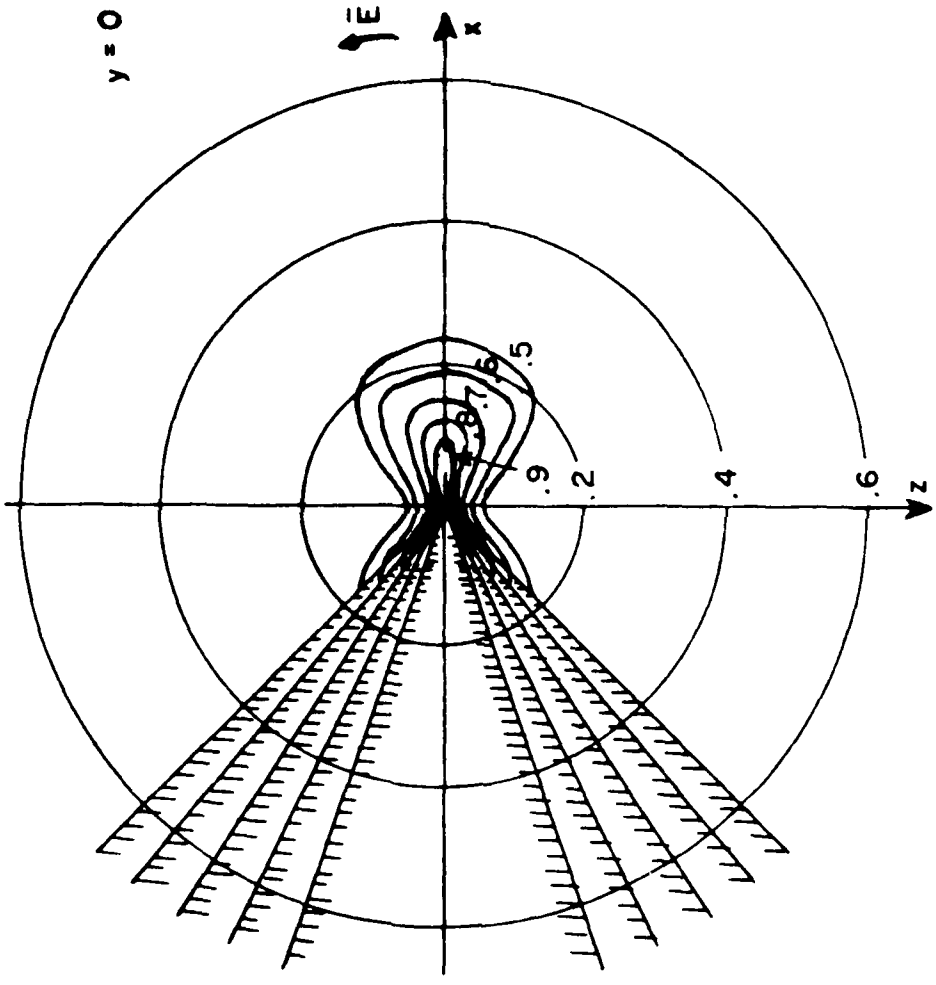

Figure 20. Total electric field for five different angular sectors.

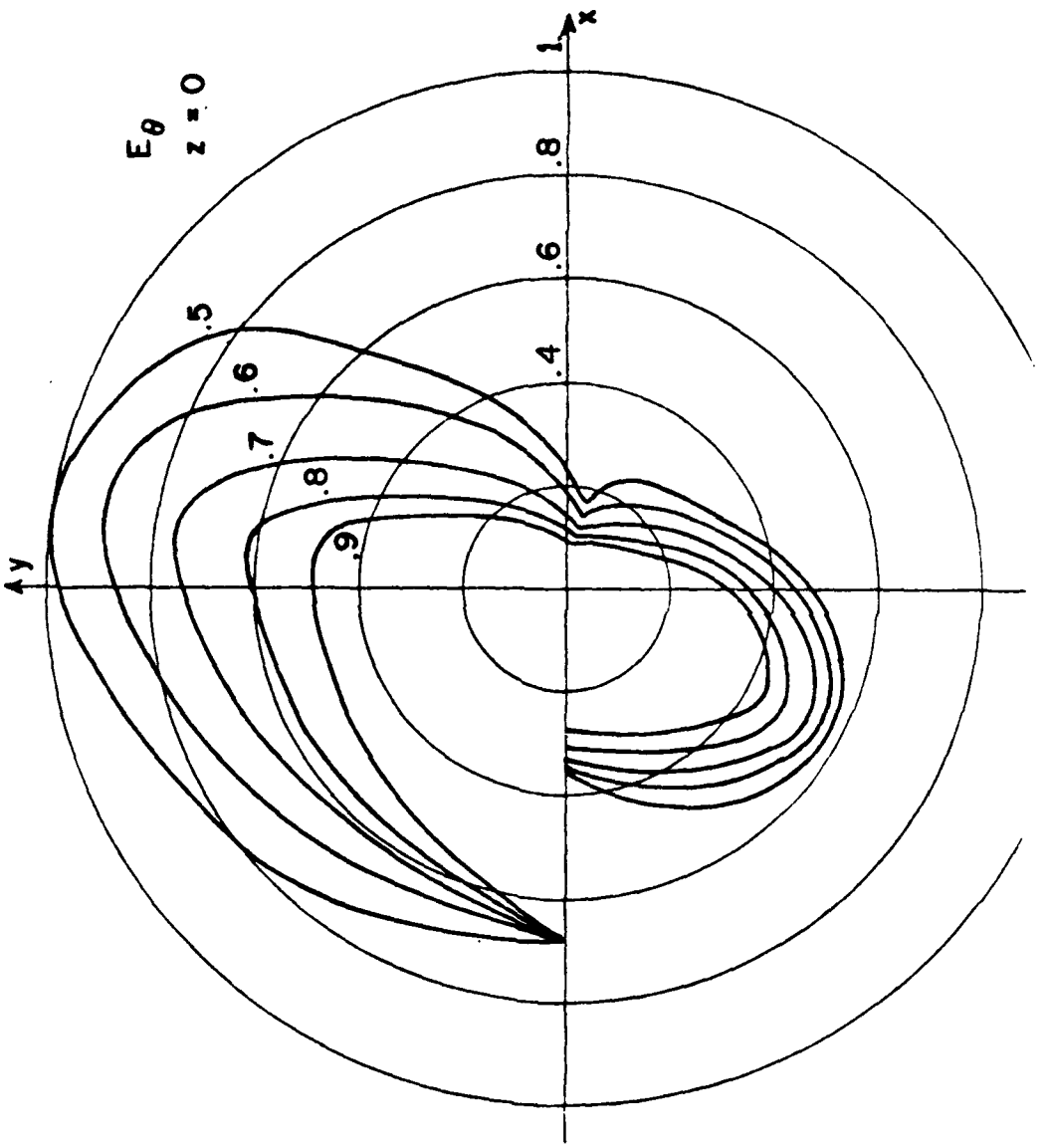

Figure 21. Total electric field for five different angular sectors.

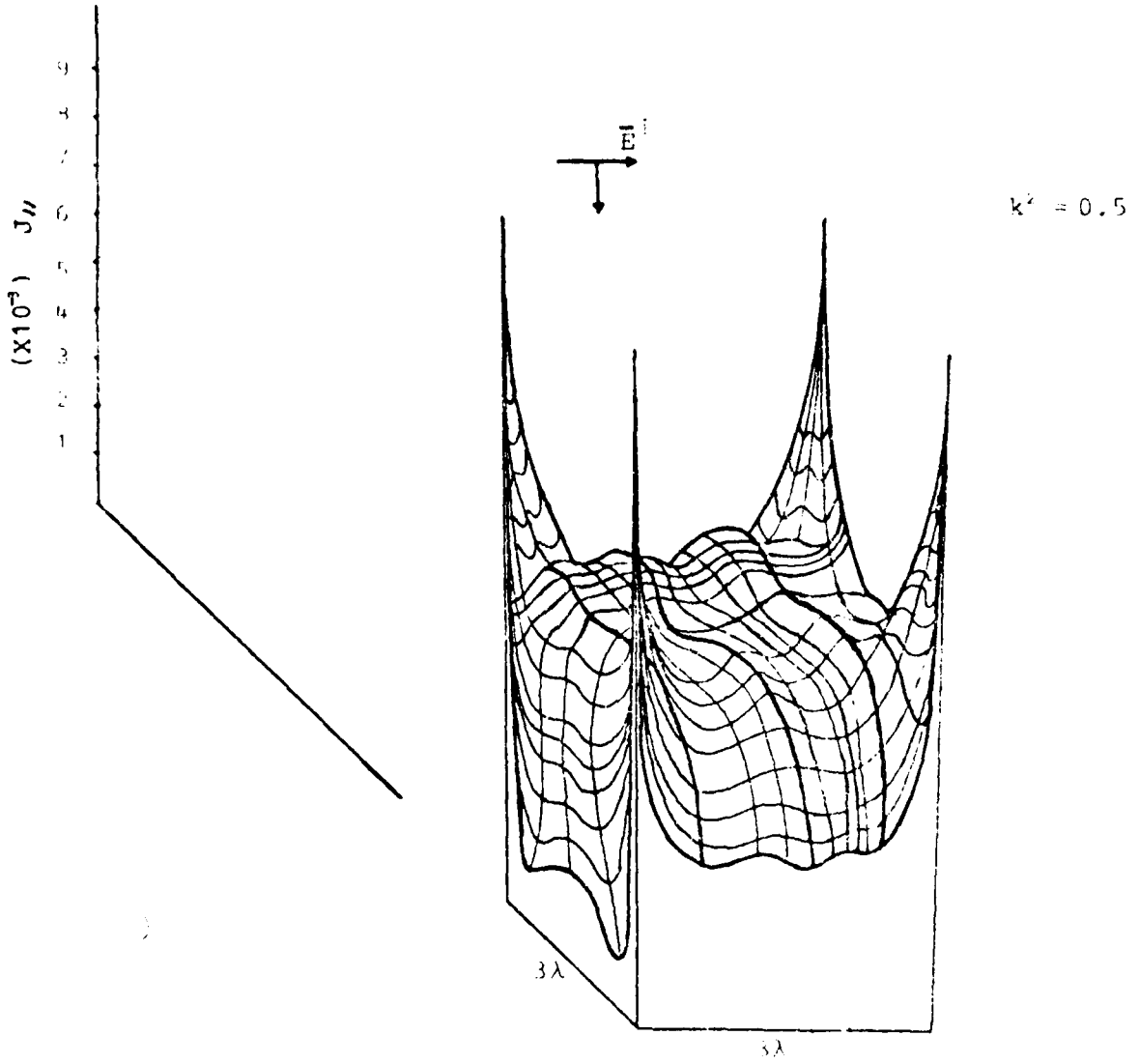

Figure 22a. Current distribution on a 3λ square plate.

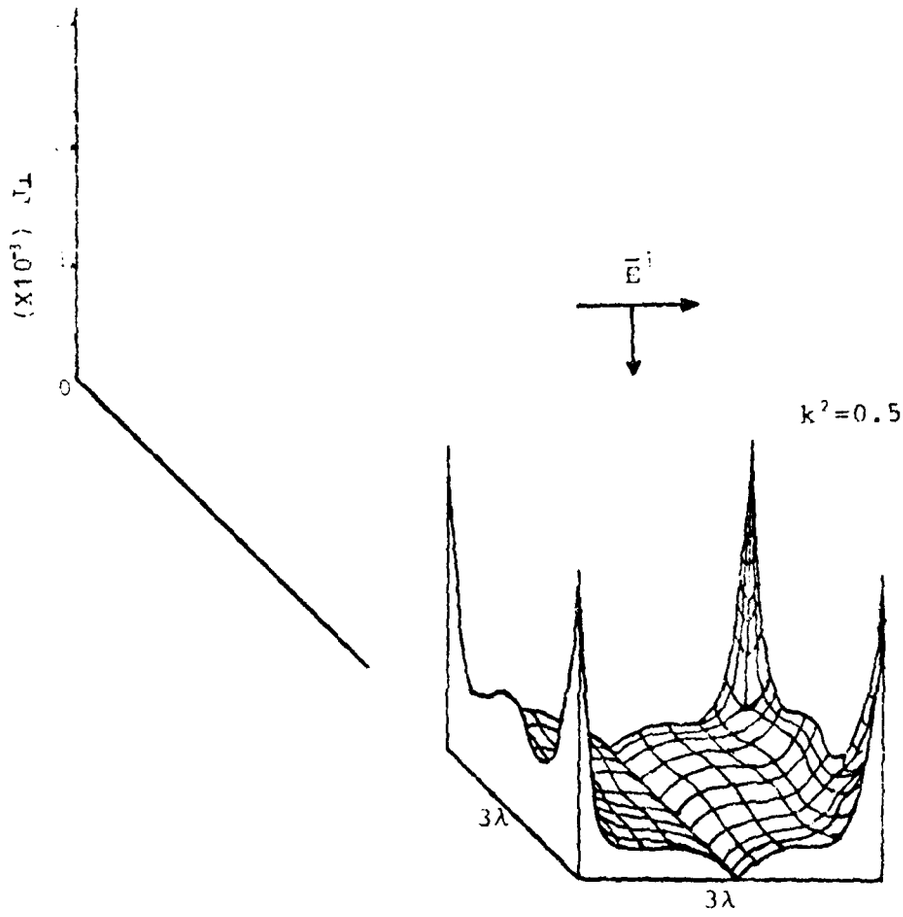

Figure 22b. Cross-polarized current on a 3λ square plate.

IX. SUMMARY

In this paper we have presented in easy to use graphical form the first few contributing eigenvalues for any angular sector having a wide range of included angle. We have shown that it is only these first few eigenvalues that contribute to the current in a region very close to the tip itself. Beyond this region the GTD may be used to obtain the current thereby overcoming the need to use large numbers of eigenvalues and eigenfunctions.

We then applied the combined eigenfunction-GTD technique to find the currents and resulting radiation fields. To demonstrate the validity of the solution, the radiation pattern of a monopole at the center of a square plate is compared with that calculated with an unpublished GTD solution which includes vertex diffraction. The two independent results are in very close agreement.

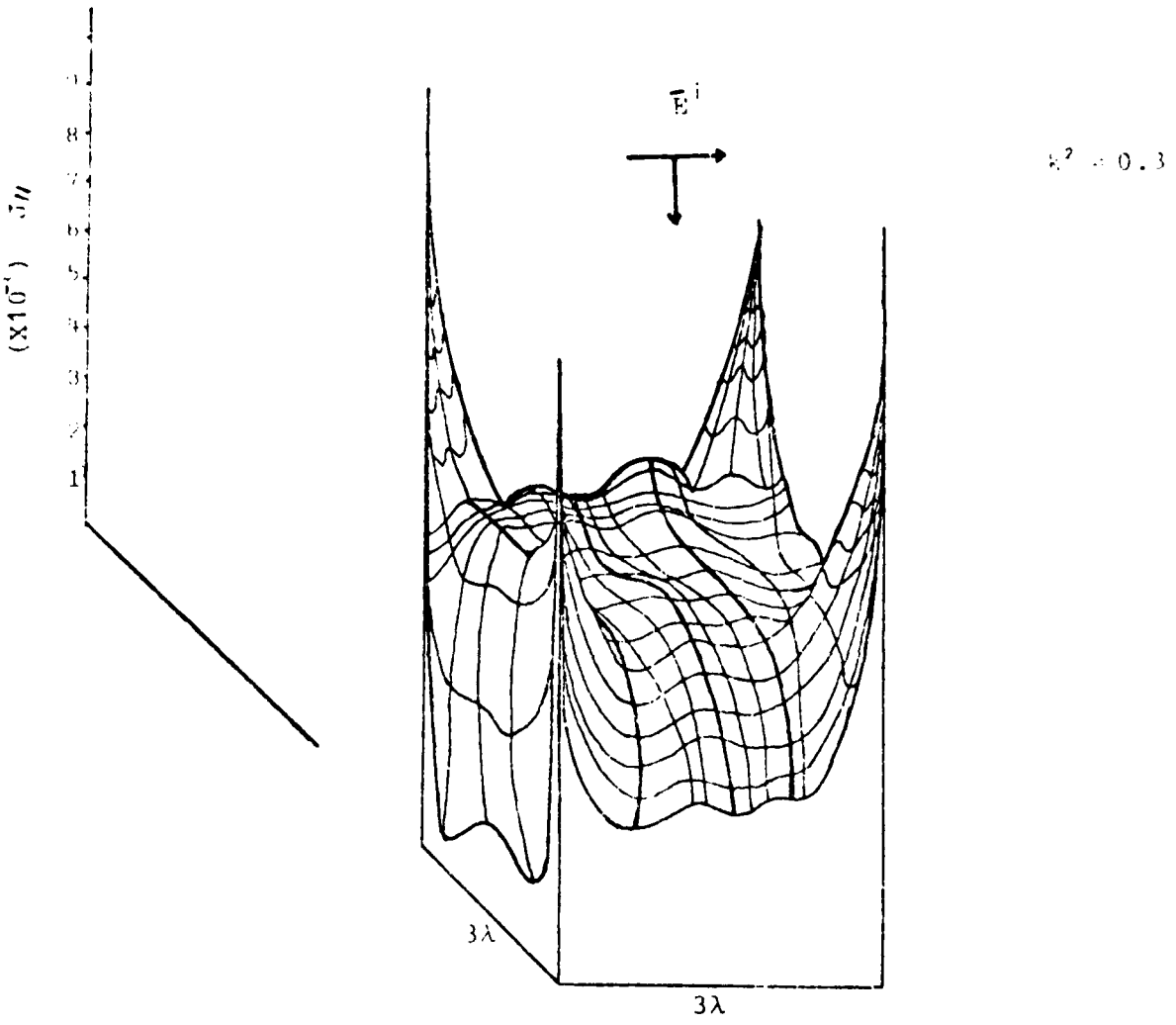

Figure 23a. Current distribution on a 3λ rhombic shaped plate.

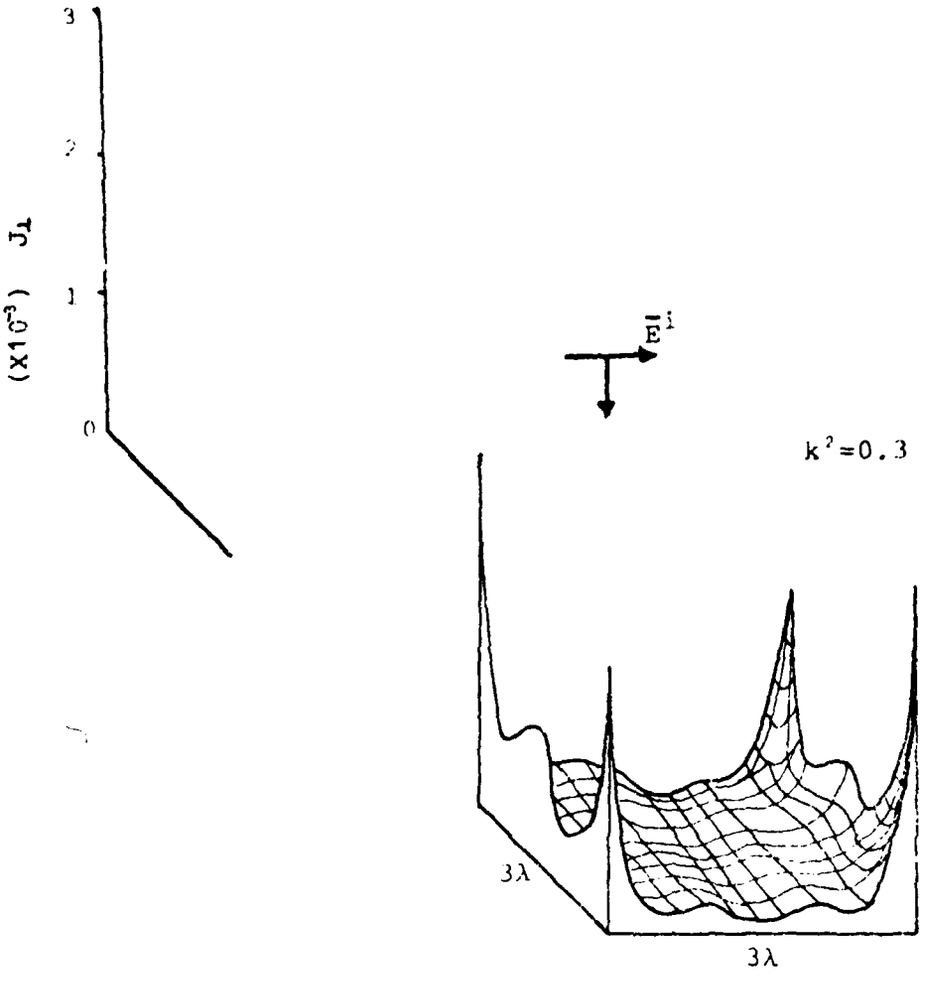

Figure 23b. Cross-polarized current on a 3λ rhombic shaped plate.

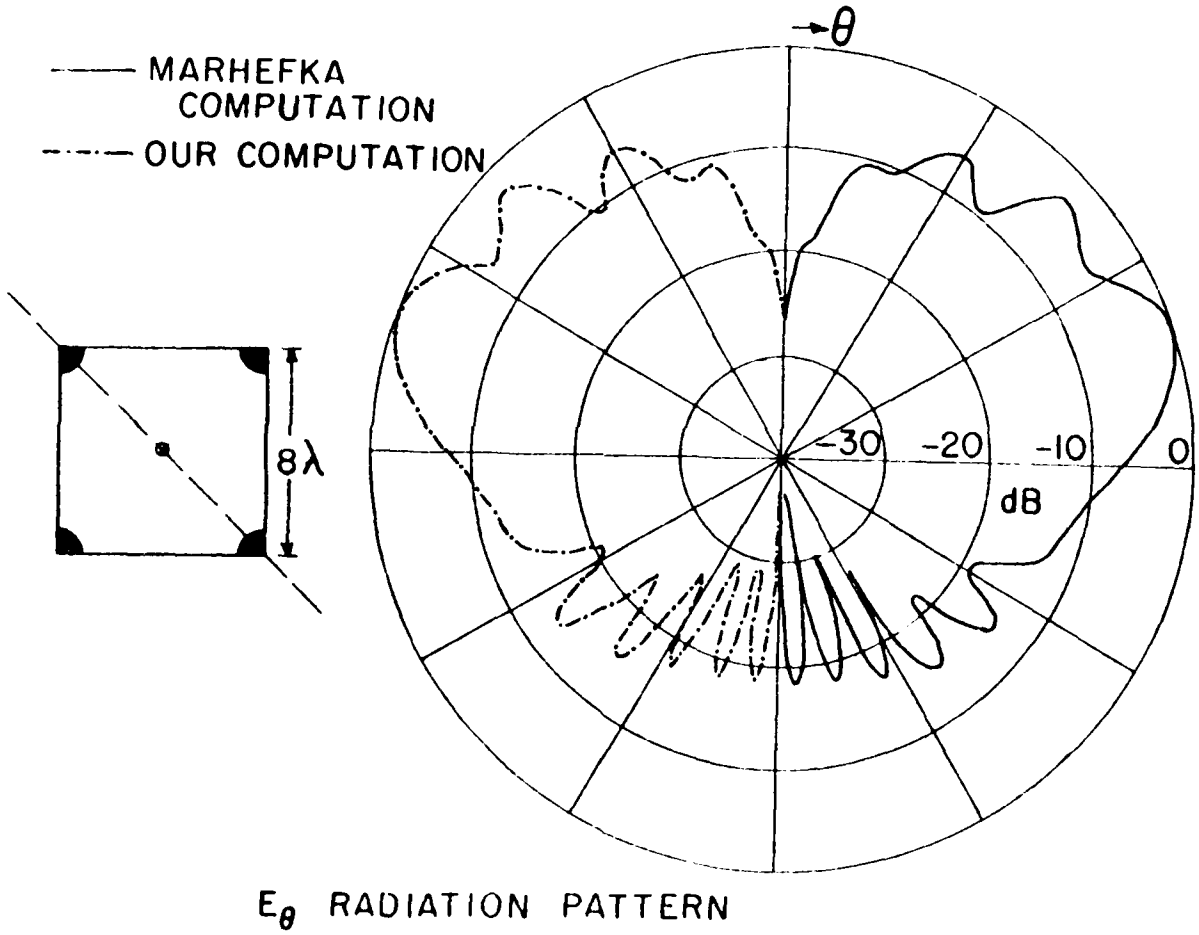

Figure 24. Far field pattern in the plane diagonally through an 8λ square plate with a short monopole in the center.

REFERENCES

1. R. Satterwhite and R.G. Kouyoumjian, "Electromagnetic Diffraction by a Perfectly-Conducting Plane Angular Sector," ElectroScience Laboratory, Ohio State University, Columbus, Ohio, Technical Report 2183-2, 1970.

2. R. Satterwhite, "Diffraction by a Quarter Plane, the Exact Solution, and Some Numerical Results," IEEE Transaction on Antennas and Propagation, AP-22, No. 3, May 1974, pp. 500-503.

3. L. Kraus, "Diffraction by a Plane Angular Sector," Thesis, New York University, 1955.

4. L. Kraus and L. Levine, "Diffraction by an Elliptic Cone," Communications on Pure and Applied Mathematics, Vol. XIV, 1961, pp. 49-68.

5. W. L. Ko and R. Mittra, "A New Approach on a Combination of Integral Equation and Asymptotic Techniques for Solving Electromagnetic Scattering Problems." IEEE Transactions on Antennas and Propagation, Vol. AP-25, Mar. 1977, pp. 187-197.

APPENDIX

The following tables give the lower order eigenvalues for angular vectors with $0.1 \leq k^2 \leq 0.9$ and for $0.0 \leq \nu \leq 1.0$ and $0.5 \leq \nu' \leq 1.5$.

Eigenvalues ν', μ'

	$k^2 = 0.9$	$k'^2 = 0.1$
ν'	μ'	μ'
0.50	-0.20000	0.93071
0.55	-0.24688	0.92820
0.60	-0.29764	0.92557
0.65	-0.35239	0.92281
0.70	-0.41125	0.91993
0.75	-0.47434	0.91692
0.80	-0.54172	0.91379
0.85	-0.61345	0.91053
0.90	-0.68959	0.90715
0.95	-0.77017	0.90364
1.00	-0.85522	0.90000
1.05	-0.94477	0.89623
1.10	-1.03884	0.89234
1.15	-1.13741	0.88832
1.20	-1.24049	0.88418
1.25	-1.34810	0.87991
1.30	-1.46022	0.87550
1.35	-1.57687	0.87096
1.40	-1.69803	0.86630
1.45	-1.82371	0.86150
1.50	-1.95396	0.85658

Eigenvalues ν', μ'

	$k^2 = 0.8$	$k^2 = 0.2$
ν'	μ'	μ'
0.50	-0.15000	0.86020
0.55	-0.19151	0.85530
0.60	-0.23614	0.85016
0.65	-0.28399	0.84477
0.70	-0.33519	0.83913
0.75	-0.38983	0.83324
0.80	-0.44801	0.82710
0.85	-0.50984	0.82071
0.90	-0.57536	0.81406
0.95	-0.64466	0.80716
1.00	-0.71778	0.80000
1.05	-0.79478	0.79258
1.10	-0.87569	0.78490
1.15	-0.96055	0.77696
1.20	-1.04938	0.76876
1.25	-1.14219	0.76029
1.30	-1.23901	0.75156
1.35	-1.33987	0.74255
1.40	-1.44472	0.73328
1.45	-1.55359	0.72373
1.50	-1.66656	0.71391

Eigenvalues ν', μ'

	$k^2 = 0.7$	$k'^2 = 0.3$
ν'	μ'	μ'
0.50	-0.10000	0.78823
0.55	-0.13622	0.78109
0.60	-0.17496	0.77358
0.65	-0.21630	0.76571
0.70	-0.26033	0.75746
0.75	-0.30715	0.74884
0.80	-0.35683	0.73984
0.85	-0.40945	0.73046
0.90	-0.46510	0.72069
0.95	-0.52385	0.71054
1.00	-0.58575	0.70000
1.05	-0.65088	0.68906
1.10	-0.71930	0.67773
1.15	-0.79102	0.66599
1.20	-0.86610	0.65385
1.25	-0.94458	0.64129
1.30	-1.02649	0.62832
1.35	-1.11184	0.61492
1.40	-1.20066	0.60110
1.45	-1.29297	0.58685
1.50	-1.38880	0.57217

Eigenvalues ν', μ'

	$k^2 = 0.6$	$k'^2 = 0.4$
ν'	μ'	μ'
0.50	-0.05000	0.71445
0.55	-0.08098	0.70524
0.60	-0.11397	0.69555
0.65	-0.14904	0.68537
0.70	-0.18625	0.67469
0.75	-0.22566	0.66352
0.80	-0.26735	0.65185
0.85	-0.31137	0.63967
0.90	-0.35781	0.62697
0.95	-0.40670	0.61375
1.00	-0.45811	0.60000
1.05	-0.51210	0.58571
1.10	-0.56873	0.57088
1.15	-0.62803	0.55550
1.20	-0.69007	0.53956
1.25	-0.75488	0.52305
1.30	-0.82252	0.50595
1.35	-0.89299	0.48828
1.40	-0.96634	0.47000
1.45	-0.04258	0.45112
1.50	-0.12176	0.43162

Eigenvalues ν', μ'

	$k^2 = 0.5$	$k'^2 = 0.5$
ν'	μ'	μ'
0.50	0.00000	0.63835
0.55	-0.02577	0.62730
0.60	-0.05312	0.61564
0.65	-0.08209	0.60339
0.70	-0.11273	0.59053
0.75	-0.14507	0.57705
0.80	-0.17916	0.56294
0.85	-0.21507	0.54819
0.90	-0.25282	0.53279
0.95	-0.29246	0.51673
1.00	-0.33405	0.50000
1.05	-0.37761	0.48258
1.10	-0.42321	0.46447
1.15	-0.47091	0.44564
1.20	-0.52070	0.42609
1.25	-0.57265	0.40580
1.30	-0.62679	0.38475
1.35	-0.68317	0.36293
1.40	-0.74180	0.34032
1.45	-0.80274	0.31690
1.50	-0.86600	0.29265

Eigenvalues ν', μ'

ν'	$k^2 = 0.4$ μ'	$k^2 = 0.6$ μ'
0.50	0.05000	0.55915
0.55	0.02941	0.54654
0.60	0.00763	0.53323
0.65	-0.01537	0.51922
0.70	-0.03963	0.50448
0.75	-0.06515	0.48900
0.80	-0.09198	0.47277
0.85	-0.12015	0.45577
0.90	-0.14968	0.43799
0.95	-0.18061	0.41941
1.00	-0.21296	0.40000
1.05	-0.24678	0.37975
1.10	-0.28208	0.35865
1.15	-0.31890	0.33665
1.20	-0.35727	0.31375
1.25	-0.39723	0.28992
1.30	-0.43879	0.26514
1.35	-0.48200	0.23937
1.40	-0.52687	0.21258
1.45	-0.57345	0.18476
1.50	-0.62177	0.15586

Eigenvalues ν', μ'

	$k^2 = 0.3$	$k'^2 = 0.7$
ν'	μ'	μ'
0.50	0.10000	0.47549
0.55	0.08458	0.46174
0.60	0.06831	0.44720
0.65	0.05116	0.43186
0.70	0.03314	0.41569
0.75	0.01423	0.39867
0.80	-0.00560	0.38078
0.85	-0.02636	0.36199
0.90	-0.04806	0.34228
0.95	-0.07073	0.32163
1.00	-0.09437	0.30000
1.05	-0.11902	0.27736
1.10	-0.14468	0.25369
1.15	-0.17137	0.22894
1.20	-0.19912	0.20308
1.25	-0.22794	0.17608
1.30	-0.25785	0.14788
1.35	-0.28887	0.11846
1.40	-0.32104	0.08776
1.45	-0.35434	0.05573
1.50	-0.38881	0.02234

Eigenvalues ν', μ'

	$k^2 = 0.2$	$k^2 = 0.8$
ν'	μ'	μ'
0.50	0.15000	0.38463
0.55	0.13973	0.37040
0.60	0.12892	0.35532
0.65	0.11756	0.33934
0.70	0.10564	0.32245
0.75	0.09317	0.30462
0.80	0.08012	0.28581
0.85	0.06650	0.26598
0.90	0.05229	0.24509
0.95	0.03750	0.22312
1.00	0.02211	0.20000
1.05	0.00611	0.17570
1.10	-0.01050	0.15017
1.15	-0.02773	0.12334
1.20	-0.04559	0.09517
1.25	-0.06409	0.06560
1.30	-0.08324	0.03456
1.35	-0.10304	0.00198
1.40	-0.12352	-0.03221
1.45	-0.14468	-0.06809
1.50	-0.16651	-0.10573

Eigenvalues ν', μ'

	$k^2 = 0.1$	$k'^2 = 0.9$
ν'	μ'	μ'_{2e_1}
0.50	0.20000	0.27916
0.55	0.19487	0.26576
0.60	0.18948	0.25147
0.65	0.18383	0.23627
0.70	0.17792	0.22011
0.75	0.17174	0.20293
0.80	0.16529	0.18469
0.85	0.15858	0.16535
0.90	0.15160	0.14483
0.95	0.14434	0.12307
1.00	0.13682	0.10000
1.05	0.12901	0.075551
1.10	0.12093	0.04964
1.15	0.11258	0.02218
1.20	0.10394	-0.00693
1.25	0.09501	-0.03778
1.30	0.08580	-0.07049
1.35	0.07631	-0.10517
1.40	0.06652	-0.14194
1.45	0.05644	-0.18094
1.50	0.04606	-0.22230

Eigenvalues ν, μ

	$k^2 = 0.9$	$k'^2 = 0.1$	$k'^2 = 0.1$
ν	μ	μ	μ
0.00	0.09283	0.00000	-0.94901
0.05	0.07531	0.00259	-0.94511
0.10	0.05568	0.00543	-0.94083
0.15	0.03365	0.00852	-0.93619
0.20	0.00917	0.01186	-0.93117
0.25	-0.01799	0.01545	-0.92577
0.30	-0.04798	0.01929	-0.92001
0.35	-0.08100	0.02339	-0.91387
0.40	-0.11723	0.02773	-0.90736
0.45	-0.15683	0.03234	-0.90047
0.50	-0.20000	0.03719	-0.89321
0.55	-0.24689	0.04230	-0.88553
0.60	-0.29764	0.04767	-0.87757
0.65	-0.35239	0.05330	-0.86919
0.70	-0.41125	0.05918	-0.86043
0.75	-0.47435	0.06533	-0.85130
0.80	-0.54172	0.07173	-0.84179
0.85	-0.61345	0.07840	-0.83191
0.90	-0.68959	0.08534	-0.82165
0.95	-0.77017	0.09253	-0.81101
1.00	-0.85523	0.10000	-0.80000

Eigenvalues ν, μ

	$k^2 = 0.8$	$k'^2 = 0.2$	$k'^2 = 0.2$
ν	μ	μ	μ
0.00	0.12105	0.00000	-0.89582
0.05	0.10400	0.00511	-0.88809
0.10	0.08502	0.01071	-0.87962
0.15	0.06393	0.01681	-0.87042
0.20	0.04074	0.02341	-0.86047
0.25	0.01527	0.03052	-0.84979
0.30	-0.01256	0.03812	-0.83836
0.35	-0.04289	0.04624	-0.82619
0.40	-0.07581	0.05488	-0.81328
0.45	-0.11147	0.06402	-0.79963
0.50	-0.15000	0.07369	-0.78522
0.55	-0.19151	0.08389	-0.77008
0.60	-0.23614	0.09461	-0.75419
0.65	-0.28399	0.10586	-0.73754
0.70	-0.33519	0.11766	-0.72015
0.75	-0.38983	0.12999	-0.70201
0.80	-0.44801	0.14288	-0.68312
0.85	-0.50984	0.15631	-0.66347
0.90	-0.57536	0.17031	-0.64307
0.95	-0.64466	0.18487	-0.62191
1.00	-0.71778	0.20000	-0.60000

Eigenvalues ν, μ

	$k^2 = 0.7$	$k'^2 = 0.3$	$k'^2 = 0.3$
ν	μ	μ	μ
0.00	0.14320	0.00000	-0.83999
0.05	0.12747	0.00753	-0.82853
0.10	0.10999	0.01581	-0.81598
0.15	0.09073	0.02482	-0.80232
0.20	0.06963	0.03459	-0.78757
0.25	0.04661	0.04511	-0.77171
0.30	0.02160	0.05640	-0.75475
0.35	-0.00549	0.06847	-0.73668
0.40	-0.03472	0.08131	-0.71751
0.45	-0.06620	0.09494	-0.69722
0.50	-0.10000	0.10937	-0.67582
0.55	-0.13623	0.12461	-0.65331
0.60	-0.17496	0.14067	-0.62968
0.65	-0.21630	0.15756	-0.60492
0.70	-0.26033	0.17529	-0.57904
0.75	-0.30715	0.19387	-0.55204
0.80	-0.35683	0.21331	-0.52390
0.85	-0.40945	0.23364	-0.49464
0.90	-0.46510	0.25485	-0.46423
0.95	-0.52385	0.27697	-0.43269
1.00	-0.58576	0.30000	-0.40000

Eigenvalues ν, μ

	$k^2 = 0.6$	$k^2 = 0.4$	$k^2 = 0.4$
ν	μ	μ	μ
0.00	0.16230	0.00000	-0.78093
0.05	0.14827	0.00985	-0.76586
0.10	0.13277	0.02067	-0.74934
0.15	0.11573	0.03249	-0.73137
0.20	0.09714	0.04531	-0.71195
0.25	0.07694	0.05915	-0.69107
0.30	0.05509	0.07401	-0.66874
0.35	0.03152	0.08991	-0.64494
0.40	0.00619	0.10687	-0.61966
0.45	-0.02096	0.12491	-0.59292
0.50	-0.05000	0.14404	-0.56470
0.55	-0.08098	0.16429	-0.53499
0.60	-0.11397	0.18566	-0.50380
0.65	-0.14904	0.20819	-0.47111
0.70	-0.18625	0.23188	-0.43693
0.75	-0.22567	0.25678	-0.40124
0.80	-0.26735	0.28289	-0.36404
0.85	-0.31137	0.31024	-0.32532
0.90	-0.35781	0.33886	-0.28508
0.95	-0.40670	0.36877	-0.24331
1.00	-0.45811	0.40000	-0.20000

Eigenvalues ν,μ

ν	$k^2 = 0.5$ μ	$k'^2 = 0.5$ μ	$k''^2 = 0.5$ μ
0.00	0.17943	0.00000	-0.71777
0.05	0.16740	0.01202	-0.69924
0.10	0.15413	0.02526	-0.67893
0.15	0.13959	0.03973	-0.65682
0.20	0.12377	0.05546	-0.63292
0.25	0.10664	0.07245	-0.60722
0.30	0.08815	0.09075	-0.57971
0.35	0.06828	0.11037	-0.55038
0.40	0.04699	0.13133	-0.51923
0.45	0.02424	0.15368	-0.48625
0.50	0.00000	0.17743	-0.45142
0.55	-0.02577	0.20263	-0.41476
0.60	-0.05312	0.22930	-0.37623
0.65	-0.08209	0.25747	-0.33584
0.70	-0.11273	0.28718	-0.29357
0.75	-0.14507	0.31848	-0.24941
0.80	-0.17916	0.35139	-0.20336
0.85	-0.21507	0.38596	-0.15541
0.90	-0.25282	0.42222	-0.10554
0.95	-0.29246	0.46022	-0.05374
1.00	-0.33404	0.50000	0.00000

Eigenvalues ν, μ

	$k^2 = 0.4$	$k'^2 = 0.6$	$k'^2 = 0.6$
ν	μ	μ	μ
0.00	0.19523	0.00000	-0.64918
0.05	0.18538	0.01401	-0.62740
0.10	0.17453	0.02947	-0.60351
0.15	0.16267	0.04639	-0.57751
0.20	0.14980	0.06483	-0.54938
0.25	0.13588	0.08480	-0.51911
0.30	0.12090	0.10634	-0.48670
0.35	0.10485	0.12951	-0.45213
0.40	0.08769	0.15433	-0.41539
0.45	0.06942	0.18086	-0.37646
0.50	0.05000	0.20914	-0.33534
0.55	0.02941	0.23922	-0.29201
0.60	0.00763	0.27115	-0.24645
0.65	-0.01537	0.30498	-0.19865
0.70	-0.03963	0.34078	-0.14859
0.75	-0.06515	0.37859	-0.09627
0.80	-0.09199	0.41849	-0.04166
0.85	-0.12015	0.46051	0.01526
0.90	-0.14968	0.50473	0.07450
0.95	-0.18061	0.55121	0.13607
1.00	-0.21297	0.60000	0.20000

Eigenvalues ν, μ

ν	$k^2 = 0.3$ μ	$k^2 = 0.7$ μ	$k^2 = 0.7$ μ
0.00	0.20999	0.00000	-0.57286
0.05	0.20246	0.01573	-0.54814
0.10	0.19418	0.03313	-0.52102
0.15	0.18514	0.05223	-0.49147
0.20	0.17535	0.07309	-0.45948
0.25	0.16478	0.09577	-0.42503
0.30	0.15343	0.12031	-0.38812
0.35	0.14128	0.14678	-0.34871
0.40	0.12834	0.17525	-0.30680
0.45	0.11458	0.20578	-0.26235
0.50	0.10000	0.23844	-0.21536
0.55	0.08458	0.27332	-0.16579
0.60	0.06830	0.31049	-0.11362
0.65	0.05116	0.35002	-0.05884
0.70	0.03314	0.39200	-0.00141
0.75	0.01423	0.43651	0.05868
0.80	-0.00560	0.48364	0.12146
0.85	-0.02636	0.53347	0.18696
0.90	-0.04806	0.58609	0.25520
0.95	-0.07073	0.64157	0.32620
1.00	-0.09438	0.70000	0.40000

Eigenvalues ν,μ

	$k^2 = 0.2$	$k^2 = 0.8$	$k^2 = 0.8$
ν	μ	μ	μ
0.00	0.22395	0.00000	-0.48428
0.05	0.21885	0.01702	-0.45714
0.10	0.21324	0.03591	-0.42732
0.15	0.20713	0.05674	-0.39480
0.20	0.20052	0.07958	-0.35956
0.25	0.19339	0.10453	-0.32157
0.30	0.18576	0.13165	-0.28081
0.35	0.17761	0.16106	-0.23723
0.40	0.16893	0.19285	-0.19082
0.45	0.15973	0.22711	-0.14154
0.50	0.15000	0.26397	-0.08936
0.55	0.13973	0.30353	-0.03423
0.60	0.12892	0.34590	0.02386
0.65	0.11756	0.39121	0.08496
0.70	0.10564	0.43951	0.14911
0.75	0.09317	0.49108	0.21634
0.80	0.08012	0.54588	0.28668
0.85	0.06650	0.60407	0.36019
0.90	0.05229	0.66575	0.43688
0.95	0.03750	0.73103	0.51681
1.00	0.02211	0.80000	0.60000

Eigenvalues ν, μ

	$k^2 = 0.1$	$k^2 = 0.9$	$k^2 = 0.9$
ν	μ	μ_{ic_1}	μ_{ic_2}
0.00	0.23725	0.00000	-0.37123
0.05	0.23466	0.01742	-0.34276
0.10	0.23182	0.03689	-0.31143
0.15	0.22873	0.05853	-0.27719
0.20	0.22539	0.08245	-0.23999
0.25	0.22179	0.10880	-0.19979
0.30	0.21794	0.13771	-0.15654
0.35	0.21384	0.16933	-0.11019
0.40	0.20948	0.20381	-0.06069
0.45	0.21487	0.24134	-0.00797
0.50	0.20000	0.28206	0.04801
0.55	0.19487	0.32615	0.10731
0.60	0.18948	0.37379	0.17000
0.65	0.18383	0.42512	0.23612
0.70	0.17792	0.48031	0.30573
0.75	0.17174	0.53952	0.37890
0.80	0.16529	0.60287	0.45568
0.85	0.15858	0.67049	0.53612
0.90	0.15160	0.74249	0.62029
0.95	0.14434	0.81897	0.70823
1.00	0.13682	0.90000	0.80000

MISSION
of
Rome Air Development Center

RADC plans and executes research, development, test and selected acquisition programs in support of Command, Control Communications and Intelligence (C^3I) activities. Technical and engineering support within areas of technical competence is provided to ESD Program Offices (POs) and other ESD elements. The principal technical mission areas are communications, electromagnetic guidance and control, surveillance of ground and aerospace objects, intelligence data collection and handling, information system technology, ionospheric propagation, solid state sciences, microwave physics and electronic reliability, maintainability and compatibility.

Printed by
United States Air Force
Hanscom AFB, Mass. 01731

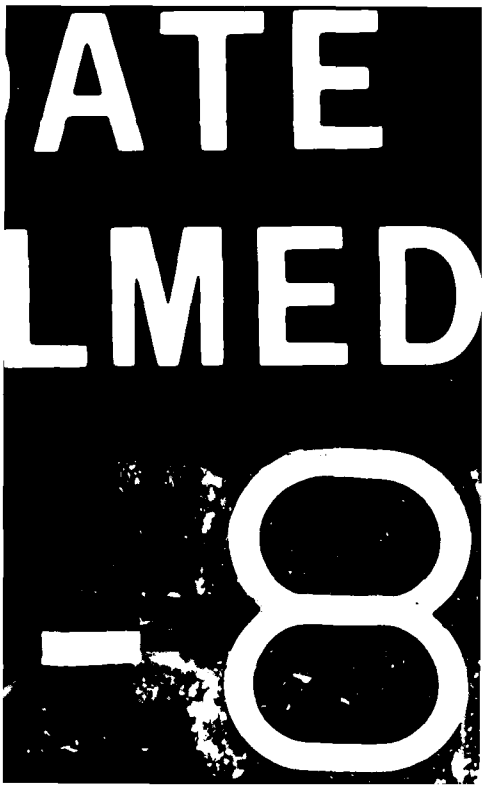
ATE
LMED
-8